Inorganic Chemistry

Article

pubs.acs.org/IC

An Extended Chain and Trinuclear Complexes Based on Pt(II)−M (M = Tl(I), Pb(II)) Bonds: Contrasting Photophysical Behavior

Juan Forniés,[†] Nora Giménez,[‡] Susana Ibáñez,[†,§] Elena Lalinde,[‡] Antonio Martín,*[,†] and M. Teresa Moreno*[,‡]

[†]Departamento de Química Inorgánica-Instituto de Síntesis Química y Catálisis Homogénea, Universidad de Zaragoza - C.S.I.C. 50009 Zaragoza, Spain

[‡]Departamento de Química-Centro de Síntesis Química de La Rioja, (CISQ), Universidad de La Rioja, 26006 Logroño, Spain

Supporting Information

ABSTRACT: The syntheses and structural characterizations of a Pt−Tl chain $[\{Pt(bzq)(C_6F_5)_2\}Tl(Me_2CO)]_n$ **1** and two trinuclear Pt_2M clusters $(NBu_4)[\{Pt(bzq)(C_6F_5)_2\}_2Tl]$ **2** and $[\{Pt(bzq)(C_6F_5)_2\}_2Pb]$ **3** (bzq = 7,8-benzoquinolinyl), stabilized by donor−acceptor Pt → M bonds, are reported. The one-dimensional heterometallic chain **1** is formed by alternate "$Pt(bzq)(C_6F_5)_2$" and "$Tl(Me_2CO)$" fragments, with Pt−Tl bond separations in the range of 2.961(1)−3.067(1) Å. The isoelectronic trinuclear complexes **2** (which crystallizes in three forms, namely, **2a**, **2b**, and **2c**) and **3** present a sandwich structure in which the Tl(I) or Pb(II) is located between two "$Pt(bzq)(C_6F_5)_2$" subunits. NMR studies suggest equilibria in solution implying cleavage and reformation of Pt−M bonds. The lowest-lying absorption band in the UV−vis spectra in CH_2Cl_2 and tetrahydrofuran (THF) of **1**, associated with ^{1}MLCT/^{1}L′LCT $^1[5d_\pi(Pt) \rightarrow \pi^*(bzq)]/^1[(C_6F_5) \rightarrow bzq]$, displays a blue shift in relation to the precursor, suggesting the cleavage of the chain maintaining bimetallic Pt−Tl fragments in solution, also supported by NMR spectroscopy. In **2** and **3**, it shows a blue shift in THF and a red shift in CH_2Cl_2, supporting a more extensive cleavage of the Pt−M bonds in THF solutions than in CH_2Cl_2, where the trinuclear entities are predominant. The Pt−Tl chain **1** displays in solid state a bright orange-red emission ascribed to ^{3}MM′CT (M′ = Tl). It exhibits remarkable and fast reversible vapochromic and vapoluminescent response to donor vapors (THF and Et_2O), related to the coordination/decoordination of the guest molecule to the Tl(I) ion, and mechanochromic behavior, associated with the shortening of the intermetallic Pt−Tl separations in the chain induced by grinding. In frozen solutions (THF, acetone, and CH_2Cl_2) **1** shows interesting luminescence thermochromism with emissions strongly dependent on the solvent, concentration, and excitation wavelengths. The Pt_2Tl complex **2** shows an emission close to **1**, ascribed to charge transfer from the platinum fragment to the thallium $[^3$(L+L′)MM′CT]. **2** also shows vapoluminescent behavior in the presence of vapors of Me_2CO, THF, and Et_2O, although smaller and slower than those of **1**. The trinuclear neutral complex Pt_2Pb **3** displays a blue-shift emission band, tentatively assigned to admixture of ^{3}MM′CT $^3[Pt(d) \rightarrow Pb(sp)]$ with some metal-mediated intraligand ($^3\pi\pi/^3$ILCT) contribution. In contrast to **1** and **2**, **3** does not show vapoluminescent behavior.

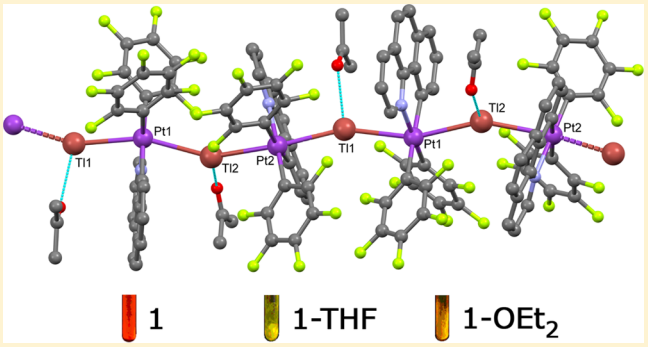

INTRODUCTION

The study of intermetallic interactions between closed-shell metals is a field of continuous interest in inorganic and organometallic chemistry.[1−11] The appeal of these interactions resides not only in their use as a powerful tool in the design of interesting supramolecular architectures[12−30] but also in their intriguing photophysical and photochemical properties.[17,31−43]

Interestingly, some of these heterometallic systems with metal−metal bonds were found to show reversible color and emission changes in response to external stimuli such as volatile organic compounds (VOCs) (vapochromic/vapoluminescence) or mechanical force (mechanochromism), with extensive applications as photofunctional materials. This behavior generally originates from molecular changes in the solid state caused by modification of metal−metal contacts, coordination or crystal inclusion of VOCs, or alteration of weak noncovalent interactions ($\pi\cdots\pi$ interactions, hydrogen bonding, C−H$\cdots\pi$ interactions).[44−48]

Within this area, a great number of systems stabilized by donor−acceptor Pt → M′ bonds have been reported.[12−17,21−24,26,27,30,49−65] Among the acceptors M′, configuration d^{10} is the most widely represented, especially Ag(I) and, to a much lesser extent, Au(I), Hg(II), and Cd(II). In contrast to these Pt(d^8) → M′(d^{10}) systems, heteropolynuclear Pt(d^8) → M′($d^{10}s^2$) (M′ = Tl(I), Pb(II))

Received: January 15, 2015
Published: April 17, 2015

DOI: 10.1021/acs.inorgchem.5b00083
Inorg. Chem. 2015, 54, 4351−4363

derivatives have been comparatively much less explored. With regard to Pt(II) → Tl(I) heteropolynuclear clusters, several structural configurations have been reported, including di (PtTl),[21,50,66−68] tri ($PtTl_2$,[69−72] Pt_2Tl,[16,56,73,74]), tetra ("paired" $(PtTl)_2$,[21,54,75−78] trigonal Pt_3Tl[29,79]), hexanuclear clusters (Pt_2Tl_4,[78,80] Pt_3Tl_3[79]), or even infinite networks.[16,74,76,78,80,81] In comparison, the number of polymetallic complexes containing Pt(II) → Pb(II) bonds is much more scarce,[17,24,48,67,82−87] and little is known about the luminescent properties of such complexes.[17,24,85] One point of interest in these systems is the stereoactivity of the $6s^2$ electron pair of the heavy ion, particularly relevant in Pb(II) systems,[88−92] which exerts a notable influence in their structures, categorized as hemi- or holodirected. Mixing of 6s and 6p orbitals leads to a stereochemically active lone pair, generating hemidirected structures with a void in the coordination sphere of the Pb(II) and lower coordination numbers, whereas symmetrical holodirected environments are usually found with high coordination numbers. It is now stablished that different degrees of activity of the lone pair produce subtle modifications of the structure and in their photophysical responses to external stimuli.[48,86,87] In spite of this, so far only a few Pt(II)−Tl(I)/Pb(II) systems form dynamic stimuli-responsive materials.[80,86,48,87]

In the course of our recent research, we developed synthetic methods for the preparation of complexes containing Pt(II) → M donor−acceptor bonds, using a platinum complex containing the cyclometalated ligand 7,8-benzoquinolinyl (bzq) as the starting material.[13,14,21,27,30,48,65,93] In particular, the anionic $[Pt(bzq)(C_6F_5)_2]^-$ fragment has allowed us to form a rare bimetallic cationic complex $[\{Pt(bzq)(C_6F_5)_2\}Cd(cyclen)]^+$ (cyclen = 1,4,7,10-tetraazacyclododecane), exclusively stabilized by a Pt → Cd bond,[14] and several bi- and trinuclear Pt−Ag complexes featuring synergistic Pt → Ag bonds[13,27,30,48,65] and η^1-C_{bzq}−Ag bonding interactions and supramolecular $\pi\cdots\pi$ interactions between the aromatic rings of the bzq ligand.

In this paper we expand our study on the ability of the synthon $[Pt(bzq)(C_6F_5)_2]^-$ to act as a precursor in the formation of complexes containing Pt → M bonds. We report here the preparation, structural characterization, and optical properties of one unexpected infinite helicoidal chain $[\{Pt(bzq)(C_6F_5)_2\}Tl(Me_2CO)]_n$ **1** and two trinuclear Pt_2M clusters $[\{Pt(bzq)(C_6F_5)_2\}_2M]^n$ ($n = -1$, M = Tl **2**; $n = 0$, M = Pb **3**), stabilized by Pt(II) → Tl(I)/Pb(II) dative bonds. The Tl(I) chain **1** displays reversible vapochromic and vapoluminescent responses to small donor solvents (tetrahydrofuran (THF) and Et_2O), likely related to the sorption/desorption of donor molecules, which modify the guest molecule coordinated to the Tl(I) ion. It also shows mechanochromic behavior, which is associated with variation of the intermetallic Pt(II)−Tl(I) separation in the chain caused by grinding. The trinuclear Pt_2Tl compound **2** shows smaller vapoluminescent behavior and slower desolvation process in comparison to **1**, whereas the Pt_2Pb compound **3** does not show response to external stimuli.

RESULTS AND DISCUSSION

Synthesis and Structural Characterization. *Complexes with Pt → Tl Bonds.* As shown in Scheme 1, the reactions of $(NBu_4)[Pt(bzq)(C_6F_5)_2]$ (**A**) with $TlPF_6$ in acetone render the neutral extended chain $[\{Pt(bzq)(C_6F_5)_2\}Tl(Me_2CO)]_n$ (**1**) or the discrete trimetallic anionic complex $(NBu_4)[\{Pt(bzq)(C_6F_5)_2\}_2Tl]$ (**2**), depending on the molar ratio of the reactants.

Scheme 1

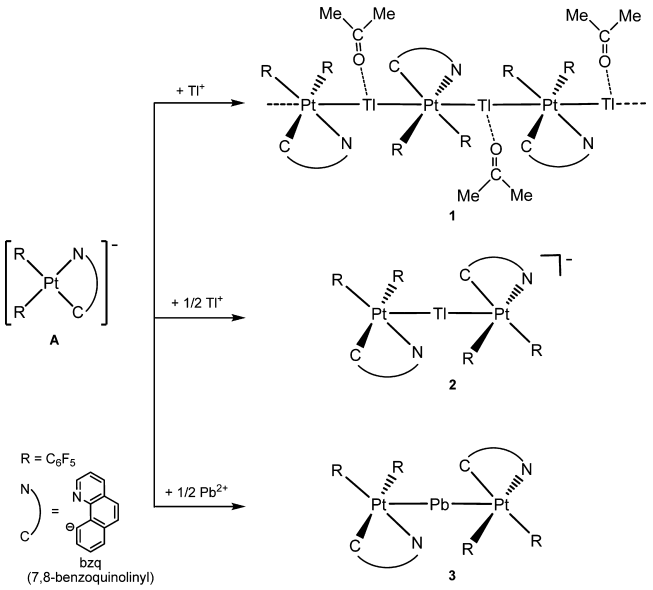

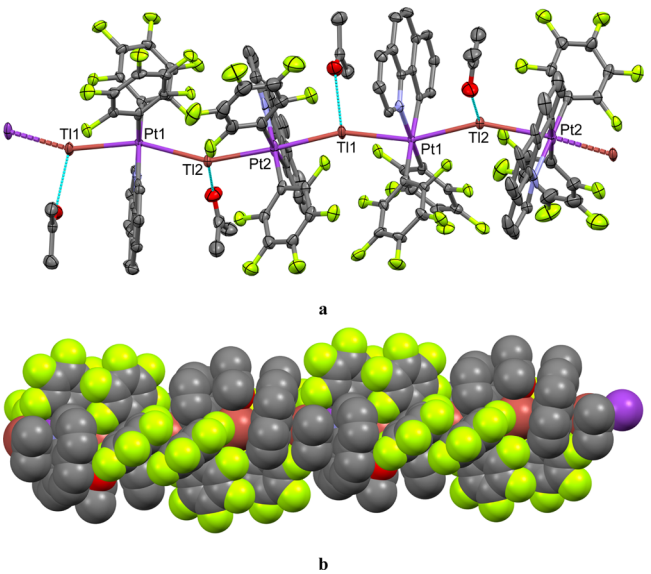

Figure 1. (a) View of the molecular structure of $[\{Pt(bzq)(C_6F_5)_2\}Tl(Me_2CO)]_n \cdot x0.5Me_2CO \cdot x0.25n\text{-}C_6H_{14}$ (**1**·$x0.5Me_2CO$·$x0.25n$-C_6H_{14}). Ellipsoids are drawn at their 50% probability level. (b) View of the helical arrangement of the infinite chain.

The crystal structure of **1** (Figure 1, Table 1, and Supporting Information, Table S1) confirms that **1** forms an infinite ···Pt−Tl−Pt−Tl··· chain with alternate "$Pt(bzq)(C_6F_5)_2$" and "Tl" fragments, which is maintained by Pt → Tl bonds. As far as we know, there is only another example of a one-dimensional heterometallic linear chain stabilized only by Pt(II)−Tl(I) bonds, without conventional bridging ligands, namely, complex $(NBu_4)_n[\{Pt(C_6F_5)_4\}Tl]_n$.[16] In **1**, the Pt−Tl distances [2.961(1)−3.067(1) Å] are similar to those found in $(NBu_4)_n[\{Pt(C_6F_5)_4\}Tl]_n$ and are in the usual range described for other Pt(II)−Tl(I) complexes with no bridging ligands

DOI: 10.1021/acs.inorgchem.5b00083
Inorg. Chem. 2015, 54, 4351−4363

Table 1. Selected Bond Lengths (Å) and Angles (deg) around the Metal (Tl or Pb) for $[\{Pt(bzq)(C_6F_5)_2\}Tl(Me_2CO)]_n \cdot x0.5Me_2CO \cdot x0.25n\text{-}C_6H_{14}$ ($1 \cdot x0.5Me_2CO \cdot x0.25n\text{-}C_6H_{14}$), $(NBu_4)[\{Pt(bzq)(C_6F_5)_2\}_2Tl]$ [$2 \cdot 0.75CH_2Cl_2$ (**2a**), $2 \cdot CH_2Cl_2$ (**2b**), and 2·THF (**2c**)], and $[\{Pt(bzq)(C_6F_5)_2\}_2Pb]$ (**3**)

	1·x0.5Me_2CO·x0.25n-C_6H_{14}		
Pt(1)−Tl(1)	2.9609(3)	Pt(1)−Tl(2)	2.9945(3)
Pt(2)−Tl(1′)	2.9301(3)	Pt(2)−Tl(2)	3.0666(3)
Tl(1)····F(1)	3.027(4)	Tl(1)····F(6)	3.057(4)
Tl(2)····F(5)	3.048(4)	Tl(2)····F(10)	3.091(3)
Tl(2)····F(15)	3.056(4)	Tl(2)····F(20)	3.083(4)
Tl(1)−O(1)	2.805(6)	Tl(2)−O(2)	2.720(5)
Pt(1)−Tl(2)−Pt(2)	150.179(11)	Pt(2′)−Tl(1)−Pt(1)	154.931(10)
Tl(1)−Pt(1)−Tl(2)	159.81(1)	Tl(1″)−Pt(2)−Tl(2)	149.091(11)
	2·$0.75CH_2Cl_2$ (**2a**)	**2**·CH_2Cl_2 (**2b**)	**2**·THF (**2c**)
Pt(1)−Tl	2.8815(4)	2.9254(3)	2.9352(6)
Pt(2)−Tl	2.9432(4)	2.8747(3)	2.9705(6)
Tl(1)····F(1)	2.976(6)	2.850(4)	3.141(3)
Tl(1)····F(10)	3.205(5)	3.201(4)	3.106(3)
Tl(1)····F(15)	2.901(6)	2.951(4)	3.154(3)
Tl(1)····F(16)	3.150(4)	3.016(3)	3.255(3)
Tl−O			2.630(4)
Pt(1)−Tl−Pt(2)	150.65(2)	146.91(1)	155.91(1)
	3		
Pt−Pb	2.7757(3)	Pt′−Pb−Pt	150.26(2)
Pb····F(1)	2.972(4)	Pb····F(6)	2.792(5)

between the atom centers.[29,68,70,71,74−77,79−81,94] The Pt−Tl vectors are nearly perpendicular to the square planar basal plane [angles 12.0(1)° and 16.4(1)°]. Each Tl center is relatively near from four *ortho*-fluorine atoms, with Tl···F_o distances [range 3.027(3)−3.083(4) Å] noticeably lower than the sum of the van der Waals radii of Tl and F (3.43 Å),[95] thus probably contributing to the final stabilization of the chain.[16,76] The environment of the Tl centers is completed by a weak interaction with the oxygen atom of an acetone molecule [Tl(1)−O(1) 2.805(6) Å, Tl(2)−O(2) 2.720(5) Å],[76,80,94,96] located between consecutive bzq planes. The existence of these Tl−O interactions seems not to affect the strength of the Pt−Tl bonds, since the intermetallic distances are comparable to that reported in the related complex $(NBu_4)_n[\{Pt(C_6F_5)_4\}Tl]_n$.[16] In contrast to the linear −[Tl−Pt]− sequence observed in this homoleptic chain, in **1** the ···Pt−Tl−Pt−Tl··· sequence is not linear [Tl(1)−Pt(1)−Tl(2) 159.81(1)°, Tl(1)−Pt(2)−Tl(2) 149.09(1)°, Pt(1)−Tl(1)−Pt(2) 154.93(1)°, Pt(1)−Tl(2)−Pt(2) 150.18(1)°]. The dihedral angles between consecutive square planes are 20.3(2)° and 17.7(2)°, respectively. The overall disposition of the molecular chain constitutes a helix, with the ligands around the Pt in the $Pt(bzq)(C_6F_5)_2$ subunits rotated about 90° with respect to their position in the previous subunit. Since the ···Pt−Tl−Pt−Tl··· wire lies essentially in a 2_1 crystallographic axis and the asymmetric unit contains a Pt_2Tl_2 fragment, one cycle of the helix is completed every four $Pt(bzq)(C_6F_5)_2$ fragments, being the length of the $(\{Pt(bzq)(C_6F_5)_2\}Tl(Me_2CO))_4$ motif of 22.98 Å. A helical motif is also found in $[\{Tl[Tl\{cis\text{-}Pt(C_6F_5)_2(CN)_2\}]_n$[76] and in the related complex $[\{Pt(bzq)(C_6F_5)_2\}Ag]_n$, with a span of 14.13 Å.[27]

As an additional note, it is noteworthy to mention that one of the bzq ligands present in an asymmetric unit is disordered over two positions, with a partial occupancy of 0.7/0.3, in such a way that the position of the nitrogen atom is inverted with respect to the other disordered representation. This disorder does not affect the essential parameters of the polymeric structure, since the rings of the two disordered dispositions of the bzq ligands are almost superimposable, and the structural data given in this text refer to the majority component of the disorder.

Complex **2** has been crystallized in three different forms (Figure 2, Table 1, and Supporting Information, Figure S1 and Table S2): two indistinguishable pseudopolymorphs[97] **2**·$0.75CH_2Cl_2$ (**2a**) and **2**·CH_2Cl_2 (**2b**), obtained by crystallization from CH_2Cl_2/*n*-hexane and the adduct **2·THF** (**2c**), obtained by crystallization from THF/*n*-hexane. The measured optical properties (absorption and emission, see below) are of the bulk material. In the three forms, the anions present a sandwich-type structure with a Tl(I) center bonded to two $Pt(bzq)(C_6F_5)_2$ fragments. However, in the form **2·THF** (**2c**) the molecule of THF is also coordinated to the Tl center [2.630(4) Å],[98−100] which is reflected in the bonding interactions with the platinum fragments. Thus, the two formed Pt → Tl bonds exhibit intermetallic distances slightly shorter in **2a** and **2b** than in **2c** [2.943(1), 2.881(1) Å **2a** and 2.925(1), 2.875(1) Å **2b** vs 2.935(1), 2.971(1) Å **2c**]. Similarly, the Pt−Tl−Pt bond sequence is not linear, the angle at the thallium center being slightly larger in the adduct **2c** [155.91(1)°] than in **2a** and **2b** [150.65(2)° **2a**, 146.91(1)° **2b**]. As in **1**, all three forms of **2** exhibit four relatively short *o*-F···Tl distances [2.900(6)−3.150(4) Å **2a**; 2.850(4)−3.200(3) Å **2b**; 3.106(3)−3.255(3) Å **2c**], which might indicate the existence of weak additional stabilizing contacts. These contacts are slightly weaker for **2c**, probably due to the extra contribution of the THF to the electronic requirements of the acidic Tl center.

A noteworthy difference between the two forms (**2a**, **2b**) crystallized from CH_2Cl_2/*n*-hexane is the different disposition of the two Pt(bzq) units. While in **2b** they adopt a relative syn disposition, in **2a** (and also in **2c**) the two Pt(bzq) units are anti to each other (see Supporting Information, Figure S1). A similar situation was found in the related complexes $[\{Pt(bzq)(C_6F_5)_2\}_2Ag]^-$,[13] $[\{Pt(bzq)(C_6F_5)L\}_2Ag]$,[30,65] and in the minor component of the disorder found in the structure of **1**. There are also differences in the supramolecular arrangement of

DOI: 10.1021/acs.inorgchem.5b00083
Inorg. Chem. 2015, 54, 4351−4363

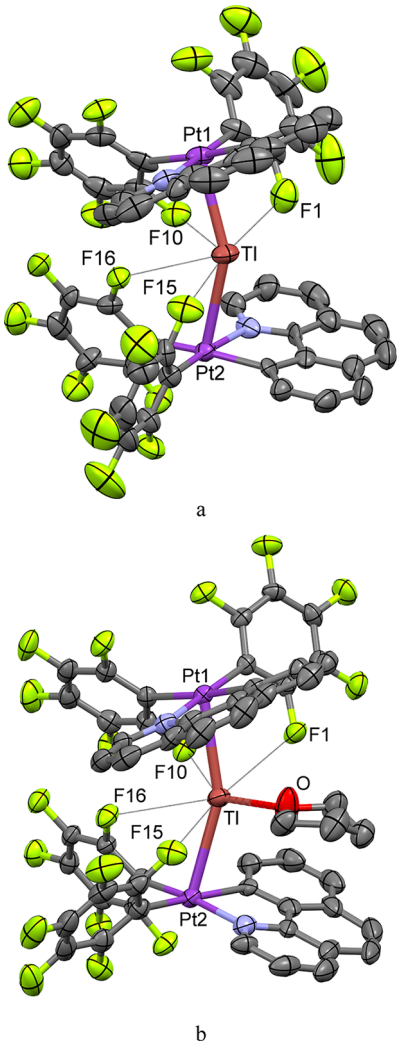

Figure 2. View of the molecular structures of the complex anion of $(NBu_4)[\{Pt(bzq)(C_6F_5)_2\}_2Tl]$ as found in the forms **2a** (a) and **2c** (b). Ellipsoids are drawn at their 50% probability level.

the $[\{Pt(bzq)(C_6F_5)_2\}_2Tl]^-$ anions. Thus, while for **2b** the bzq ligands of two neighbor anion complexes stack with an interplanar distance of ca. 3.6 Å, establishing weak $\pi\cdots\pi$ interactions and forming dimers in a similar way to other Pt(bzq) complexes (see Supporting Information, Figure S1c),[13,14,17,30,65,101−106] neither **2a** nor **2c** show these interactions. This is because the NBu_4^+ cations locate just in front of the external face of the bzq ligands, preventing other anions from coming close.

Complexes **1** and **2** were fully characterized by analytical and spectroscopic techniques, and their integrity in solution was studied by multinuclear (^1H, ^{19}F (CD_3COCD_3, CD_2Cl_2), and $^{195}Pt\{^1H\}$) NMR spectroscopy. The matrix-assisted laser desorption ionization (MALDI(+)) mass spectrum of **1**, using DCTB in acetone as matrix, gave the fragmentation peaks corresponding to the Pt−Tl fragments $[Pt(bzq)(C_6F_5)_2Tl(CH_3COCH_3)]^+$ (*m*/*z* 957, 40%) and $[Pt(bzq)(C_6F_5)_2Tl_2]^+$ (*m*/*z* 1116, 12%). In its MALDI(−) spectrum appear the peaks corresponding to $[Pt(bzq)(C_6F_5)_2]^-$ (*m*/*z* 707) and $[\{Pt(bzq)(C_6F_5)_2\}_2Tl]^-$ (*m*/*z* 1620). The MALDI spectra for **2** show in (+) mode the Pt−Tl fragments $[Pt(bzq)Tl(CH_3COCH_3)]^+$ (*m*/*z* 623) and $[Pt(bzq)(C_6F_5)_2Tl(CH_3COCH_3)]^+$ (*m*/*z* 957), whereas in (−) mode the peak associated with $[Pt(bzq)(C_6F_5)_2]^-$ (*m*/*z* 707). These spectra might suggest a fragmentation of the complexes in solution via partial rupturing of Pt···Tl bonding interactions. Indeed, the molar conductivity in acetone gives a value of 48 Ω^{-1} cm^{-2} mol^{-1} for **1**, in accordance with a partial dissociation of the Pt−Tl bond, and 118 Ω^{-1}cm^{-2} mol^{-1} for **2**, corresponding to a 1:1 electrolyte.

Additional relevant information was obtained from ^{19}F NMR spectroscopy. Thus, in CD_3COCD_3, complex **1** exhibits signals compatible with the existence of two AA′MM′X spin systems, in accordance with the inequivalence of the two C_6F_5 ligands on the platinum fragments. The *ortho*-fluorine resonances are seen down-field (by 0.5 ppm, C_6F_5 trans to C) and up-field (by 1.6 ppm, C_6F_5 trans to N) shifted, respectively, in comparison to the precursor, thus supporting the presence of fragments having Pt−Tl bonds in solution. Significantly, the ^{195}Pt−*o*-F coupling constants are notably smaller than those in the starting precursor (223 and 426 Hz **1** vs 310 and 580 Hz **A**), which is consistent with the increase in the coordination number upon formation of Pt−Tl bonds. At low temperature (198 K), both *o*-fluorine signals broaden, indicating a dynamic behavior. The $^{195}Pt\{^1H\}$ NMR spectrum (CD_3COCD_3) shows a singlet notably deshielded in relation to the precursor (−2826 **1** vs −3705 ppm **A**), further supporting the presence of Pt−Tl bonds in solution. In addition, the lack of an observable coupling between Pt and Tl atoms also suggests that the Pt−Tl bond is dynamic on the NMR time scale. Addition of successive amounts of $TlPF_6$ to a solution of complex **1** at room temperature only causes a negligible reduction of the $^3J_{o\text{-F−Pt}}$ coupling constants (from 223, 420 to 219, 415 Hz, Supporting Information, Figure S2), whereas addition of successive amounts of starting material $(NBu_4)[Pt(bzq)(C_6F_5)_2]$ (**A**) produces a displacement of the *o*-F signals with a concomitant increase of the $^3J_{o\text{-F−Pt}}$ coupling constants (Supporting Information, Figure S3). When 1 equiv of **A** is added, **2** is formed (Scheme 2i), but no signals for pure **A** are observed.

Scheme 2

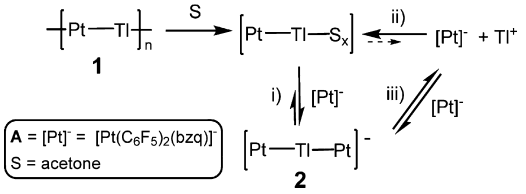

These spectra are consistent with the equilibria shown in Scheme 2. It is suggested that dissolution of the chain **1** in acetone mainly occurs as solvated bimetallic $[Pt(bzq)(C_6F_5)_2Tl(S_x)]$ fragments, which are additionally involved, in low extent, in a fast equilibrium with the anionic precursor via cleavage of the Pt−Tl bond (Scheme 2ii). The ^{19}F NMR spectra of **1** in CD_2Cl_2 reveal a more rigid behavior (see Supporting Information, Figure S4). At room temperature, the para and meta (broad) fluorine resonances are observed, whereas the *ortho*-F do not raise from the baseline, indicative of dynamic behavior. Unfortunately, its low solubility prevented obtainment of good NMR spectra at low temperature in this solvent.

For complex **2**, we observed that the data (δ and $^3J_{o\text{-F−Pt}}$) obtained of their ^{19}F NMR spectra in CD_3COCD_3 depend on the concentration, which is also consistent with a dynamic behavior. As shown in Supporting Information, Figure S5,

DOI: 10.1021/acs.inorgchem.5b00083
Inorg. Chem. 2015, 54, 4351−4363

dilution of a solution from 8.9×10^{-3} M to 1×10^{-4} M causes a progressive shift of the signals of the F_{ortho} and a concomitant increase of the $^{3}J_{o\text{-}F-Pt}$ (from 250 to 265 Hz and 480 to 510 Hz; data given for 1×10^{-3} M in the Experimental Section). In any case, the $^{3}J_{o\text{-}F-Pt}$ coupling constants are smaller than in **A**, confirming the presence of Pt−Tl bonds in solution (also supported by the ^{195}Pt{^{1}H} NMR, −3052 **2** vs −3705 ppm **A**). At low temperature (198 K), only broadening of the two *o*-fluorine signals was observed. When successive amounts of **A** are added to a solution of **2**, a displacement of the signals toward those observed for **A** takes place, thus confirming the occurrence of a fast equilibrium between **2**, **A**, and Tl^{+} (Scheme 2iii), which averages the chemical shifts corresponding to **2** and **A** (Supporting Information, Figure S6). In the same way as for **1**, the coupling constants increase with the additional incorporation of **A** in solution. The ^{19}F NMR spectra of **2** were also recorded in CD_2Cl_2, revealing a more rigid behavior than in acetone (broader signals) and persistence of Tl···F contacts in solution (Supporting Information, Figure S7). At 298 K, **2** shows two sets of AA′MXX′ patterns (as in acetone). When the temperature is lowered, the *o*-F signals broaden and coalesce at 238 K, and at 198 K a rigid pattern for a trinuclear species with the Tl(I) interacting with four nonequivalent *o*-fluorine atoms is observed. A very broad resonance appears at δ −117.1 ppm, due to the *o*-F exo atoms, whereas the *o*-F endo atoms give rise to four extensive doublets due to the short contacts ^{203,205}Tl···F. Unfortunately, the corresponding coupling constants cannot be calculated, because only the external signals of the doublets are clearly visible, as the internal are overlapped with the *exo*-F signal.

Complexes with Pt → Pb Bonds. As said above, in comparison with Tl, the reports of complexes containing Pt(II) → Pb(II) dative bonds are scarce.[17,24,48,83,85,86] As it was noted by Balch et al. some years ago,[82] Pb(II) seems to be much less prone to establish this kind of interaction than Tl(I). However, complex $(NBu_4)[Pt(bzq)(C_6F_5)_2]$ (**A**) seems to be an adequate precursor for the preparation of polynuclear complexes with Pt → Pb donor−acceptor bonds. Indeed, the reaction of **A** with $PbClO_4{\cdot}3H_2O$ in 2:1 molar ratio in acetone renders, after workup of the resulting solution, the complex $[\{Pt(bzq)(C_6F_5)_2\}_2Pb]$ (**3**) as a yellow-orange solid. The crystal structure of this complex determined by X-ray diffraction is shown in Figure 3. Table 1 and Supporting Information, Table S3 list its more relevant bond lengths and angles. As can be seen, **3** is a trinuclear type "sandwich" complex very similar to $[\{Pt(bzq)(C_6F_5)_2\}_2Ag]^{-}$ [1 3] or $[\{Pt(bzq)(C_6F_5)_2\}_2Tl]^{-}$ (**2**). The complex contains two Pt → Pb bonds unsupported by any conventional bridging ligand, the Pt−Pb distances being 2.776(1) Å, in the range found for the similar Pt−Pb complexes mentioned above.[17,24,83,85,86] This distance is shorter than those found in the forms of **2** $[\{Pt(bzq)(C_6F_5)_2\}_2Tl]^{-}$ [**2a**−**2c**, range from 2.875(1) to 2.973(1) Å, vide supra], and a similar trend has been previously observed in the isolectronic homoleptic anions $[\{Pt(C_6F_5)_4\}_2Tl]^{3-}$ [Pt−Tl 2.978(1), 3.043(1) Å][16] and $[\{Pt(C_6F_5)_4\}_2Pb]^{2-}$ [Pt−Pb 2.769(2), 2.793(2) Å].[83] This structural feature can be attributed to the smaller size of the ion Pb(II) in relation to Tl(I),[107] taking into account that these systems usually display a notable electrostatic contribution to the M−M′ bonding interactions.[108] The Pt−Pb−Pt angle is 150.26(2)°, similar to the isostructural Tl(I) forms of **2** [146.91(1)−155.9(1)°], leading to a void in the opposite hemisphere, indicative of some steroactivity of the $6s^2$ lone pair on the M. The formation of bent Pt−M−Pt unit contrasts with

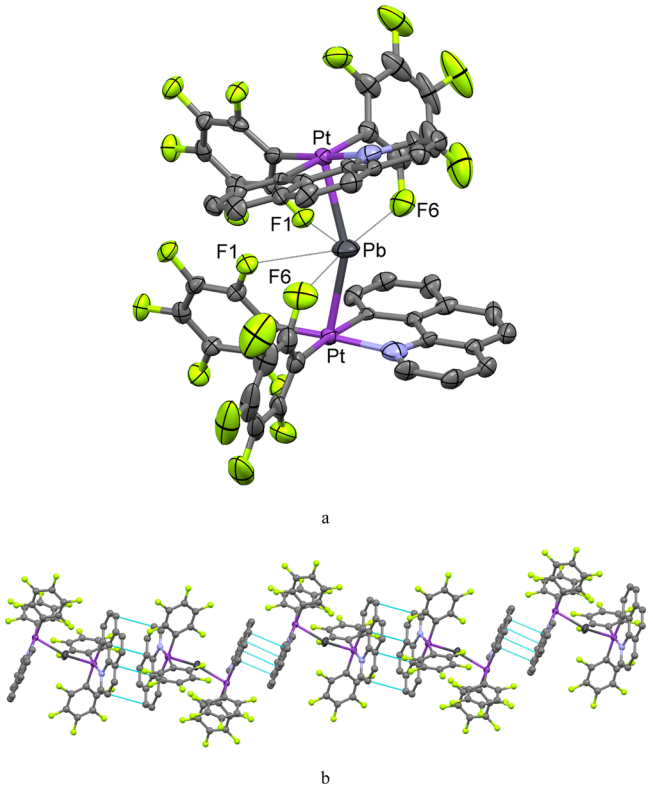

Figure 3. (a) View of the molecular structure of $[\{Pt(bzq)(C_6F_5)_2\}_2Pb]$ (**3**). Ellipsoids are drawn at their 50% probability level. (b) Supramolecular arrangement in an infinite chain of **3**.

the almost linear arrangement displayed by the homoleptic anions $[\{Pt(C_6F_5)_4\}_2Tl]^{3-}$ [Pt−Tl−Pt 174.01(2)°][16] and $[\{Pt(C_6F_5)_4\}_2Pb]^{2-}$ [Pt−Pb−Pt 178.6(1)°],[83] respectively. In these latter, the Pb(II) or Tl(I) ion achieves a holodirected bicapped antiprismatic environment with additional eight *o*-F contacts (four of each Pt fragments). By contrast, in **3** (and also in **2**), the lower charge on the platinum atoms and the planarity of the aromatic ancillary bzq ligand in the platinum units seem to play a key role in the final hemidirected coordination at the M (Pb(II) or Tl(I)) ions. Indeed, as in **2**, the environment of the Pb center in **3** is supplemented by secondary contacts with the four *endo ortho* fluorine atoms of C_6F_5 ligands [2.972(4) Å F(1), 2.792(5) Å F(6)]. The shorter *o*-F···Pb distances in **3** with respect to those *o*-F···Tl in the analogous forms of **2** are in accordance with the smaller intermetallic Pt−Pb separation.

The $[\{Pt(bzq)(C_6F_5)_2\}_2Pb]$ units arrange in the crystal structure in such a way that the bzq plane is parallel to the bzq plane of a neighboring anion, resulting in an infinite stacking of anions related by $\pi-\pi$ interactions (~3.4 Å; see Figure 3b), contrasting with the stacking in pairs found in the anions **2b** and **2c**.

The MALDI(+) mass spectrum of **3** shows the peak corresponding to the fragment $[Pt_2(bzq)_2(C_6F_5)_3Pb]^{+}$ (m/z 1454), together with the peak corresponding to $[Pt(bzq)(C_6F_5)_2Pb]^{+}$ (m/z 913). In agreement, the molar conductivity measurements in acetone for this neutral derivative give a value of 35 Ω^{-1} cm^{-2} mol^{-1}, suggesting some degree of dissociation via breaking of Pt···Pb bonding interactions. The ^{1}H NMR spectrum of **3** shows signals for only one type of bzq ligand, while the ^{19}F NMR spectrum in CD_3COCD_3 at 298 K shows two types of C_6F_5 groups, with typical AA′MM′X spin systems, indicating that the Pt coordination is a symmetry plane in the

DOI: 10.1021/acs.inorgchem.5b00083
Inorg. Chem. 2015, 54, 4351−4363

NMR time scale. As in the previous complexes, the equivalence of the two *o*-F of the same group can take place by rotation of the C_6F_5 ligands around the Pt−C_{ipso} bonds or by cleavage and reformation of the Pt−Pb bonds. In any case, the low solubility of **3** in acetone-d_6 (or CD_2Cl_2) prevents further studies of the ^{19}F NMR spectra at variable temperature.

Photophysical Properties. *Absorption Spectra.* UV−vis spectra data in solution and in solid state (diffuse reflectance) of complexes **1**−**3** and the previously published starting material **A** are summarized in Table 2. The analysis of the

Table 2. Absorption Data for Compounds 1−3 at 298 K

compound	λ_{abs}, nm ($\varepsilon \times 10^3/M^{-1}$ cm^{-1}) (solution $\approx 5 \times 10^{-5}$ M)
$(NBu_4)[Pt(bzq)(C_6F_5)_2]$ (**A**)	243 (46.9), 262 (40.3), 317 (11.0), 352 (8.4), 399 (5.6), 448 (2.5) **THF**[27]
	243 (66.4), 260 (58.4), 315 (27.5), 345 (20.1), 380 (12.1), 425 (6.9) **CH_2Cl_2**[13]
	265, 310, 357, 392, 434, 472 **solid**[27]
$[\{Pt(bzq)(C_6F_5)_2\}Tl(Me_2CO)]_n$ (**1**)	240 (28.8), 283 (12.6), 307 (9.5), 373 (2.9), 415 (1.8) **THF**
	235 (47.5), 302 (19.6), 367 (6.6), 410 (3.6) **CH_2Cl_2**
	256, 306, 412, 480, 505, 530sh, 550sh, tail to 600 **solid**
$(NBu_4)[\{Pt(bzq)(C_6F_5)_2\}_2Tl]$ (**2**)	260 (30.0), 311 (11.1), 353 (7.5), 406 (4.8) **THF**
	235 (50.1), 264 (40.1), 308 (14.0), 343 (9.0), 391 (5.0), 430 (2.5) **CH_2Cl_2**
	268, 309, 360, 430, 462sh, tail to 540 **solid**
$[\{Pt(bzq)(C_6F_5)_2\}_2Pb]$ (**3**) (**3**)	238 (30.6), 283 (11.1), 310 (8.5), 338 (6.6), 367 (3.4), 416 (1.6) **THF**
	237 (58.4), 284 (26.4), 315 (19,6), 354 (12.0), 386 (8.4),440 (5.7), 511 (2.7), tail to 555 **CH_2Cl_2**
	245, 305, 365, 437, 455, 480sh, 515sh, tail to 540, **solid**

absorption profile of the extended PtTl complex **1** dissolved in THF and in CH_2Cl_2 indicates that the extended chain dissolves probably as bimetallic fragments $[\{Pt(bzq)(C_6F_5)_2\}TlS_n]$ (S = solvent) with donor solvent molecules coordinated to the thallium center, which is also suggested by NMR spectroscopy and mass spectrometry (see above). It shows high-energy ^{1}IL absorptions (range of 240−373 nm) and a less intense band (415 nm THF, 410 nm CH_2Cl_2) ascribed, with reference to previous spectroscopic work and theoretical calculations in related binuclear complexes $[\{Pt(bzq)(C_6F_5)_2\}Ag(L)]$ (L = PPh_3, tht)[13,27] and in the extended chain $[\{Pt(bzq)(C_6F_5)_2\}Ag]_n$,[27] to an admixture of metal-to-ligand $^1[5d_\pi(Pt) \rightarrow \pi^*(bzq)]$ and ligand-to-ligand $^1[(C_6F_5) \rightarrow bzq]$ charge-transfer transitions (Figure 4). This low-energy band is blue-shifted in relation to the precursor **A** in THF (415 **1** vs 448 nm **A**) and in CH_2Cl_2 (410 **1** vs 425 nm **A**). This fact is consistent with the predominance of bimetallic fragments with a Pt−Tl donor−acceptor bond, which increases the electrophilicity of the Pt center and lowers the energy of the highest occupied molecular orbital (HOMO), resulting in an increase of the energy gap of the ^{1}MLCT $^1[Pt(d) \rightarrow \pi^*(bzq)]$ transition.

The absorption spectra of the trinuclear complexes **2** and **3** in THF solutions also exhibit a blue shift in the low-energy absorption maxima in relation to **A** (406 **2** and 416 **3** vs 448 nm **A**, THF; see Figure 4), whereas in CH_2Cl_2 they show a notable

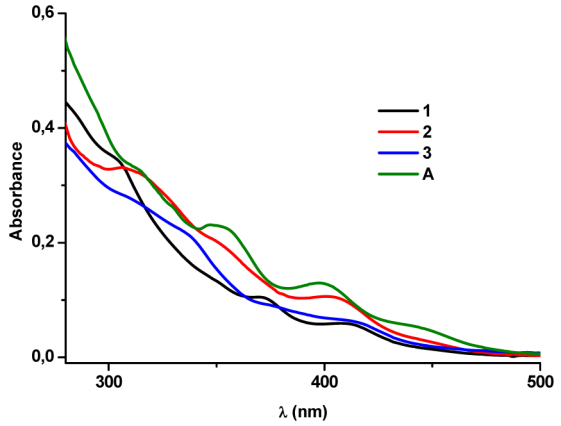

Figure 4. Absorption spectra of **1**−**3** and precursor **A** in THF 5×10^{-5} M at 298 K.

red shift, more marked in the Pt_2Pb derivative (430 **2** and 440, 511 **3** vs 425 nm **A**, CH_2Cl_2; see Supporting Information, Figure S8). The different behavior of **2** and **3** in both solvents could be associated with a more extensive cleavage of the Pt−M (M = Tl, Pb) bonds in THF solution than in CH_2Cl_2 solution in which the trinuclear entities could be predominant. For complex **2**, this fact is supported by the NMR spectroscopy at variable temperature (see above, Supporting Information, Figure S7), whereas for **3**, which is more insoluble, is also suggested by mass spectrometry and by the similarity between the absorption spectra in CH_2Cl_2 and in the solid state (diffuse reflectance, Supporting Information, Figure S9). Probably, the presence of two Pt−M bonds in the trinuclear entity decreases the contribution from the bzq ligand and increases the metallic character (Pt/M) of both the HOMO and the lowest unoccupied molecular orbitals with respect to those of the starting material. The change in the frontier orbitals modifies the nature of the low-lying absorptions from a typical ^{1}MLCT in THF to a metal−metal charge transfer (^{1}MM′CT) in CH_2Cl_2, which is consistent with the observed red shift. The effect of the increasing metallic character (Pt/Ag) in the frontier orbitals in the trinuclear Pt_2Ag derivatives $[\{Pt(bzq)(C_6F_5)L\}_2Ag]ClO_4$ (L = tht, MeCN, CN^{t}Bu, CN-Np) in relation to the binuclear PtAg derivatives $[\{Pt(bzq)(C_6F_5)L\}AgL']ClO_4$ (L = PPh_3, L′ = $pyPh_2$; L = CN^{t}Bu, CN-2,6-Me_2Ph, L′ = PPh_3) was recently confirmed by time-dependent density functional theory calculations.[30,65]

The solid-state diffuse reflectance spectrum of the extended chain **1** exhibits a characteristic low-energy feature (500−600 nm; see Supporting Information, Figure S9), which is clearly absent in the precursor and in the trinuclear derivatives **2** and **3**. This feature is tentatively assigned, as in the extended chain $[\{Pt(bzq)(C_6F_5)_2\}Ag]_n$,[27] to an admixture of ^{1}LMM′CT $^1[Pt(bzq) \rightarrow Tl]$ and ^{1}L′M′CT $^1[(C_6F_5) \rightarrow Tl]$, involving the promotion of electron density from platinum $Pt(bzq)(C_6F_5)$ fragments to the thallium center. For complexes **2** and **3**, the spectra are similar to those in CH_2Cl_2 solution, suggesting that the $\pi\cdots\pi$ intermolecular interactions observed in the solid state have a very small effect, if any, in the lowest-energy absorption maxima. The feature in the region of 430−540 nm is greatly enhanced in comparison to the precursor **A**, which correlates well with the existence of two Pt−M (M = Tl, Pb) bonds.

Emission Spectra. All complexes are brightly emissive in the solid state (Table 3), in glassy solutions and in degassed CH_2Cl_2 solutions at 298 K (Supporting Information, Table S4),

DOI: 10.1021/acs.inorgchem.5b00083
Inorg. Chem. 2015, 54, 4351−4363

Table 3. Photophysical Data for Complexes 1−3 in Solid State

compound	T, K	λ_{em}, nm (λ_{exc}, nm) [ϕ/%]	τ, μs	K_r[a]	K_{nr}[b]
1	298	610 (365−480) [28.4]	0.2 (66%), 0.6 (34%)	8.5×10^5	2.1×10^6
1	77	685 (400−480)	10.0		
1-grinding	298	665 (420−450) [2.4]	0.1 (20%), 0.7 (80%)	4.1×10^4	1.7×10^6
1-grinding	77	685 (420−450)	8.6 (11%), 2.9 (89%)		
1-THF	298	560 (365−420) [19.3]	0.1 (37%), 0.9 (63%)	3.2×10^5	1.3×10^6
1-THF	77	618 (420)	10.8 (7%), 2.9 (93%)		
1-Et_2O	298	577 (420) [44.4]	1.1 (41%), 0.4 (59%)	6.5×10^5	8.1×10^5
1-Et_2O	77	617 (420)	10.3 (46%), 3.6 (54%)		
2	298	615 (400−450) [31.7]	1.5	2.1×10^5	4.5×10^5
2	77	512, 554, 640_{max} (440)	41.1 (512)		
		640 (480)	11.0		
2-Me_2CO	298	595 (420) [30.3]	0.3	1.0×10^6	2.3×10^6
2-Me_2CO	77	615 (440)	9.6		
2-THF	298	590 (420) [0.4]	0.2	2.0×10^4	5.0×10^6
2-THF	77	595−605 (440)	21.0 (38%), 132.6 (62%) (605)		
2-Et_2O	298	588 (420) [20.1]	2.1	9.6×10^4	3.8×10^5
2-Et_2O	77	590[c] (440)	9.5		
3	298	547 (365−450) [20]	0.02 (44%), 0.5 (56.1%)	6.9×10^5	2.8×10^6
3	77	547 (365−450)	61.7		

[a] $K_r = \phi/\tau_{average}$. [b] $K_{nr} = (1 - \phi)/\tau_{average}$. [c] The weak band at 512 nm is still observed.

except **3**, for which no emission is detected in solution at room temperature (see below).

Solid State. The extended [−Pt−Tl−Pt−Tl−] chain **1** exhibits in the solid state at 298 K a bright (ϕ = 28.4%) orange-red phosphorescent emission (610 nm), which is significantly red-shifted when cooled to 77 K (685 nm), pointing to the important metallic (Pt, Tl) contribution from the Pt−Tl bonds to the frontier orbitals (^{3}MM′CT) (Figure 5). This behavior is

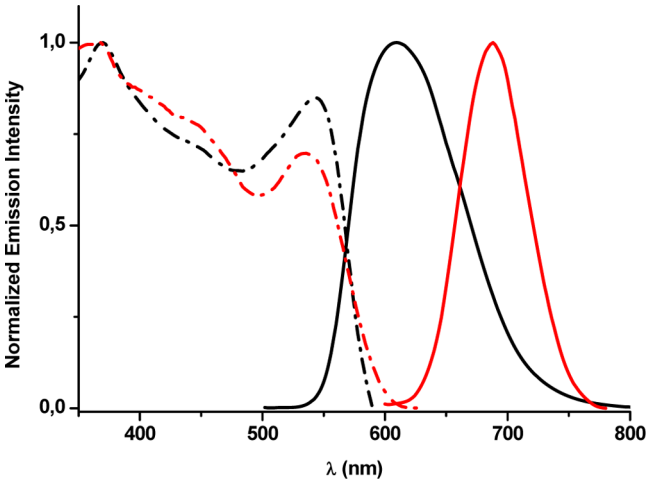

Figure 5. Normalized excitation and emission spectra of complex **1** in solid state at 298 K (black) and at 77 K (red) (λ_{exc} 400 nm).

consistent with a decrease in the Pt−Tl separation caused by thermal contraction, a phenomenon that has many precedents in extended metal···metal chain systems.[109,110] At 298 K, the emission decay was best fitted to two components [0.2 (66%), 0.6 μs (34%)], which might be attributed to small different arrangements,[48] as evidenced in its X-ray diffraction analysis. The lifetime increases remarkably at 77 K (10 μs), a feature generally attributed to the suppression of thermally activated nonradiative process. By comparison, the homoleptic $(NBu_4)_n[\{Pt(C_6F_5)_4\}Tl]_n$ displays a blue-shifted emission, both at 298 (582 nm, τ = 11.6 μs) and at 77 K (635 nm, τ = 12.6 μs).[16]

At room temperature, the emission profile of the as-obtained solid trinuclear Pt_2Tl derivative **2** is similar to that of the extended chain **1** with its maximum barely shifted to lower energies (λ_{max} 615 nm). Despite the presence of pseudopolymorphs in the crystals (see above), the emission decay of the crude solid fits to one component of 1.5 μs, and the measured quantum yield (ϕ = 31.7%) is slightly higher than that in **1**. At 77 K, the emission clearly resolves into two bands: a weak high-energy (HE) feature (λ_{max} 512 nm) and an intense, symmetrical low-energy (LE) band (λ_{max} 640 nm), with its maximum red-shifted with respect to that at 298 K (Supporting Information, Figure S10). The HE structured emission, with a long lifetime of 41.1 μs, is assigned to typical ^{3}IL/^{3}MLCT emission from the platinum fragments, whereas the LE band with shorter lifetime (11 μs) is ascribed to excited state with strong metallic contribution. The emission in **2** is notably red-shifted in relation to those of the related trinuclear derivatives $(NBu_4)_3[\{Pt(C_6F_5)_4\}_2Tl]$ (450 nm, 298 K; 445 nm, 77 K)[16] and $[Tl_2Pt(CN)_4]$ (448 nm),[69] which were attributed to a metal-centered phosphorescence process $[Pt(5dz^2)\rightarrow Tl(6p_z)]$ (^{3}MM′CT) within the trinuclear entity. The observed shift in **2** might be attributed to the presence of slightly stronger Pt−Tl bonds, as deduced by comparing intermetallic distances (2.8747(3)−2.9705(6) Å $[\{Pt(bzq)(C_6F_5)_2\}_2Tl]^-$ vs 2.9777(4), 3.0434(4) Å $[\{Pt(C_6F_5)_4\}_2Tl]^{3-}$, 3.140(1) Å $[Tl_2Pt(CN)_4]$), and mainly to the contribution of the planar and low-lying cyclometalated bzq ligand to the frontier orbitals, which likely reduces the gap of the transition. The emission is tentatively ascribed to charge transfer from the platinum fragments to the thallium [^{3}(L+L′)MM′CT].

Despite that the Pt−Pb bond distance in **3** is shorter than those of Pt−Tl in **2**, the emission of complex Pt_2Pb **3** in solid state at 298 K appears blue-shifted (λ_{max} = 547 nm, ϕ = 20%) in relation to **2**. The energy maximum remains essentially unchanged at 77 K (Supporting Information, Figure S11), but the measured lifetime increases significantly (61.7 μs) in relation to 298 K [0.02(44%), 0.5 (56.1%) μs], pointing to a

DOI: 10.1021/acs.inorgchem.5b00083
Inorg. Chem. 2015, 54, 4351−4363

higher degree of intraligand contribution. This emission can be compared to that observed in the trinuclear complex $(NBu_4)_2[\{Pt(C_6F_5)_4\}_2Pb]$ (539 nm, τ = 9 μs, 298 K; 529 nm, τ = 35 μs, 77 K),[17] which was attributed to phosphorescence of the $^3(d\sigma^*p\sigma)$ excited state, related to the linear trinuclear Pt−Pb−Pt entity. Considering this result and also previous works on heteropolynuclear bzq/C_6F_5 Pt^{II}−Pb complexes,[17,48,87] the emission in **3** is tentatively ascribed to metal-centered charge transfer ^{3}MM′CT ^{3}[Pt(d)→Pb(sp)] mixed with metal-mediated intraligand ($^3\pi\pi$/^{3}ILCT) contribution, as supported by the relatively long lifetime and the chain packing observed in the crystal structure (Figure 3b).

Vapochromic, Vapoluminescent, and Mechanochromic Properties. The as-obtained orange-red powder **1** shows the same color and luminescence as in the crystalline form $[\{Pt(bzq)(C_6F_5)_2\}Tl(CH_3COCH_3)]_n$. Addition of a drop of MeOH or MeCN has no visual effect in the color or the emission, whereas addition of CH_2Cl_2 provokes a very quick change to yellow but an immediate recovering of the initial orange color. However, the treatment of powder **1** with a drop of THF or Et_2O (fresh **1-THF** and **1-Et$_2$O** solvates) causes color and luminescence changes that can be studied. Thus, when **1** was treated with a drop of THF, a color change occurred from orange-red to yellow under ambient light, and the bright orange-red luminescence turned to yellow under UV light (Figure 6). This behavior is reflected in a blue shift in the

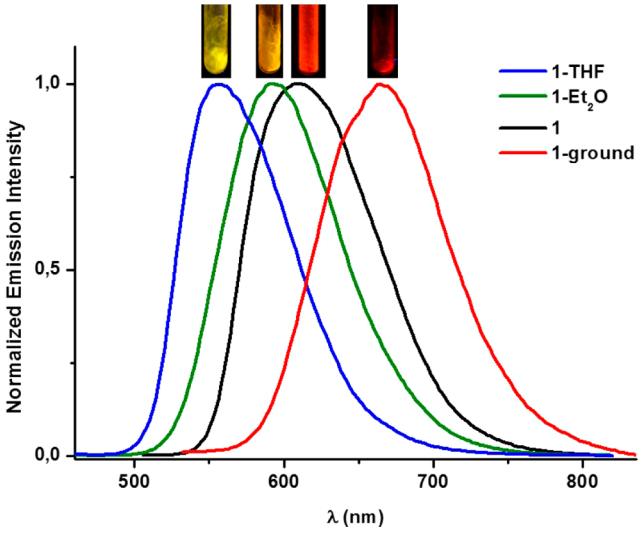

Figure 6. Normalized emission spectra of the orange-red solid **1**, **1-ground** and those of the fresh **1-THF** and **1-Et$_2$O** solvates.

emission spectra both at 298 K (610→560 nm, ϕ = 19.3%) and at 77 K (685→618 nm). The solid **1** and the fresh solvates **1-THF** and **1-Et$_2$O** display different excitation spectra, giving rise to similar Stokes shifts (~2250 **1**, 1985 **1-THF**, 2100 cm^{-1} **1-Et$_2$O**). On standing under ambient conditions, the THF is gradually lost (1 h, 580 nm 298 K; 630 nm 77 K, Supporting Information, Figure S12), showing the sample an emission at 600 nm after 12 h. A fresh **1-Et$_2$O**-solvate (Supporting Information, Figure S13) also shows color change to yellow and a significant blue shift of the emission to 577 nm at room temperature (617 nm, 77 K). On standing, the diethyl ether is also lost, recovering the sample its initial orange-red color (1 h, 605 nm, 298 K, 660 nm 77 K; 12 h, 617 nm, 298 K, 680 nm 77 K). Similar responses in color and in luminescence were observed when solid **1** was exposed to THF and Et_2O vapors at 298 K, indicating that the transformation to **1-THF** or **1-Et$_2$O** adducts occurred. After exposure of solid **1** for 30 min to THF vapors, the color and the emission change (λ_{max} 560 nm), whereas **1** exposed to diethyl ether vapor requires only 10 min to change the solid-state color and luminescence (λ_{max} = 577 nm). In this case, the emission efficiency is notably enhanced (ϕ = 44.4%) in relation to the pristine solid **1**, which is associated with a remarkable reduction in the nonradiative constants (Table 3).

Desolvation by passing of a stream of acetone or air onto the adduct samples showed the reversibility of this behavior. Upon exposure of **1-THF** to air for 5 min produces change of color and emission (from 560 to 600 nm), keeping the same emission spectra after 20 min. By passing of a stream of acetone, the luminescence changes to 580 nm in 1 min and to 610 nm in 20 min, recovering the **1-acetone** solvate, being the limit of change. The same desolvation process of **1-Et$_2$O** adduct requires ~10 min, both in air (λ_{max} ≈ 600 nm) and in acetone vapor (λ_{max} = 610 nm). It is reasonable to conclude that the oxygen donor solvents similar to acetone (THF, Et_2O) are able to contact the Tl^I center in a way similar to that described for $[\{Pt(bzq)(C_6F_5)_2\}Tl(CH_3COCH_3)]_n$ **1**, which explains the different color and emission observed. We also found that this extended chain exhibited a notable mechanochromic behavior. Thus, after the orange solid was ground, the resulting red powder showed a red shift in its emission spectra (λ_{max} 665 nm 298 K, 685 nm 77 K) with a remarkable decrease in its quantum yield (ϕ = 2.4%). The notable red shift in the crushed powder at room temperature suggests a shortening in the metal−metal separation in the chain caused by grinding.

We also observed that the as-obtained solid **2** (precipitated in acetone) shows small changes (from 615 to 595 in acetone, 590 in THF, 588 in Et_2O) in the emission maxima upon treatment with a drop of the corresponding donor solvent or vapors (~10 min, acetone; ~15 min, THF; ~1 h, Et_2O; see Figure 7 and Table 3). The emission of **2** upon treatment with THF vapors coincides with that of crystals of the adduct **2·THF** (see X-ray). The measured lifetimes of the likely formed solvates are in the same range as that of **2**, but the emission efficiencies decrease, particularly for **2-THF** (0.4% **2-THF**, 20.1% **2-Et$_2$O**, 30.3% **2-**

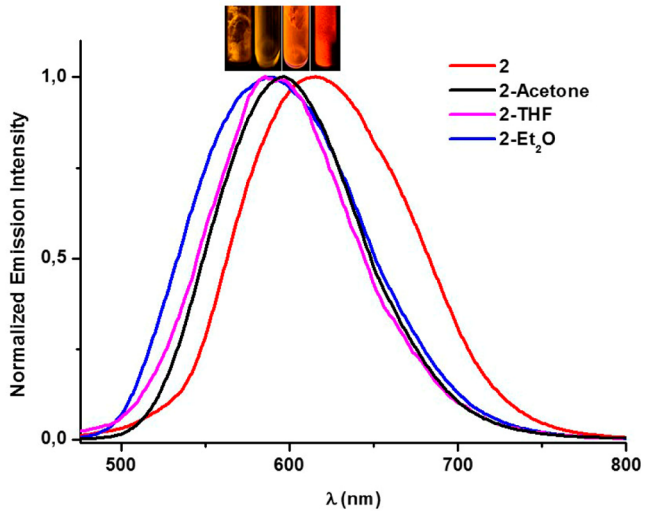

Figure 7. Normalized emission spectra of the orange solid **2** and of the solvates (**2-solvent**).

DOI: 10.1021/acs.inorgchem.5b00083
Inorg. Chem. 2015, 54, 4351−4363

Me_2CO vs 31.7% **2**), for which both the K_r and K_{nr} decrease and increase by 1 order of magnitude, respectively. The desolvation process, when passing a stream of air onto the samples **2-Me_2CO**, **2-THF**, or **2-Et_2O**, monitored using emission spectroscopy, showed that the process is slow, precluding its possible use as a sensor.

In contrast to the behavior commented, the changes in the color and in the emission color of **3** by treatment of a drop or exposure to vapors of donor solvents such as MeCN, THF, or Et_2O are negligible. We observed neither color nor significant emission changes by crushing the solid in a ceramic mortar.

Solution. Although **1** is not good emitter in solutions at 298 K, it becomes brightly emissive at 77 K (see Supporting Information, Table S4). In glassy solutions (77 K), the color and the emissions are dependent on the solvent, concentration, and excitation wavelength, exhibiting thermochromism. In concentrated THF solutions (1×10^{-3} M, deep orange glasses), **1** displays a broad low-energy emission band (600 nm). However, upon dilution, different bands are observed depending on the wavelength used for excitation (5×10^{-4} M, pale orange glasses, bands in the range from 485 to 640 nm; 5×10^{-5} M, white glasses, emission bands in the range from 480 to 590 nm). Similar behavior is observed in CH_2Cl_2 (purple glasses) and in acetone (orange to white glasses), giving rise the lowest-energy emissions in CH_2Cl_2 (λ_{max} 690 nm). To illustrate this, the emission spectra of **1** in THF at concentrations from 1×10^{-3} to 5×10^{-5} M and at several excitation wavelengths are shown in Figure 8. The observed change in the colors of glasses

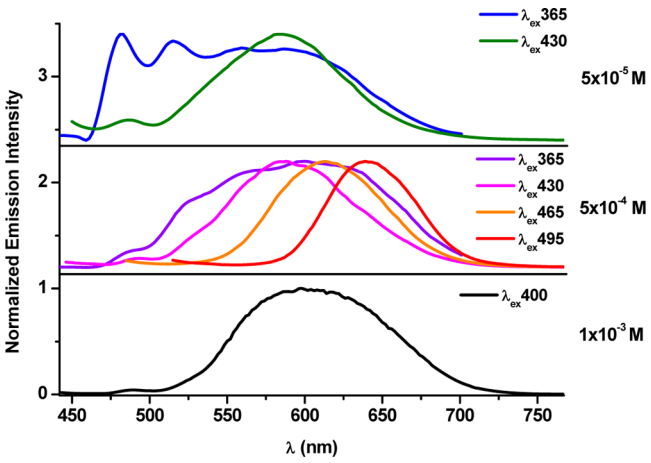

Figure 8. Normalized emission spectra of complex **1** in THF at 77 K at several concentrations (1×10^{-3}, 5×10^{-4}, and 5×10^{-5} M) and using different excitation wavelengths.

indicates that this behavior probably results from changes in the size of the aggregates formed (in the frozen process) and the Pt···Tl distances within the aggregates in the ground state. As expected, the formation of extended aggregates that emit at similar energies or even lower energies than in the solid is favored in the most concentrated solutions and using low-energy wavelength of excitation. The structured HE emission (~480 nm) resembles the emission of the precursor **A** (485, 522, 565, 611_{sh} THF, 77 K; 485, 521, 563, 608_{sh} CH_2Cl_2, 77 K) being, therefore, ascribed to mixed ^{3}MLCT/^{3}LC of the platinum fragments, whereas the intermediate multiple emissions are mainly attributed to admixture of ^{3}MM′CT/^{3}ILCT excited states on multiple discrete ground (or excimeric) $[\{Pt(bzq)(C_6F_5)_2\}_2Tl]_x^-$ units.

The room-temperature yellow solutions of **2** in CH_2Cl_2 shows an unstructured band centered at 610 nm, similar to that observed in solid state, suggesting the integrity of the trinuclear $[Pt_2Tl]^-$ anions in solution (Supporting Information, Figure S14). This emission band in fluid media is slightly red-shifted in relation to that observed in glassy solution (λ_{max} 570 nm). The occurrence of rigidochromism in heteropolynuclear complexes has many precedents[111] and has been ascribed to the larger structural changes that are more accessible in solution than in rigid media. As in the solid state, a minor high-energy feature at 487 nm is also observed in glassy media (Supporting Information, Figure S14).

The trinuclear Pt_2Pb derivative **3** is only emissive in glassy solutions. In diluted (5×10^{-5} M) CH_2Cl_2 glass two bands with different intensities (525 minor, 570 nm major) and different excitation spectra were obtained (Supporting Information, Figure S15). By increasing the concentration to 5×10^{-4} M, the minor band decreases, which indicates again the formation of two different ground-state observing species. It is worth noting that the major low-energy feature, attributed to emission in the trinuclear Pt_2Pb unit (^{3}MM′CT/^{3}ILCT), is notably red-shifted with respect to the emission in solid at 77 K (547 nm), probably due to the occurrence of intermolecular $\pi\cdots\pi$ interactions between the chromophores Pt_2Pb.

CONCLUSIONS

In summary, we report the synthesis and structures of a Pt−Tl chain $[\{Pt(bzq)(C_6F_5)_2\}Tl(Me_2CO)]_n$ (**1**) and two novel isoelectronic trinuclear Pt_2M [M = Tl(I), Pb(II)] complexes, stabilized by donor−acceptor Pt→M bonds. NMR studies suggest the occurrence of equilibria in solution implying breaking and reformation of Pt−M bonds. The UV−vis absorption spectra support this fact in the chain **1** in THF and CH_2Cl_2, in which bimetallic Pt−Tl fragments seem to be predominant, and in **2** and **3** in THF, exhibiting a blue shift in the low-energy absorption band in relation to the precursor. In a less donor solvent (CH_2Cl_2) **2** and **3** show, however, a notable red shift in the low-energy absorption, which is associated with the predominance of the trinuclear units.

The Pt−Tl compounds **1** and **2** show bright orange-red emissions with very close maxima in both. This emission is mainly ascribed to platinum-to-thallium charge transfer (^{3}MM′CT) in **1**, with some additional contribution of the ligands [^{3}(L+L′)MM′CT] (L = bzq, L′ = C_6F_5) in **2**. The trinuclear Pt_2Pb complex **3** displays a yellow emission band, tentatively ascribed to admixture of ^{3}MM′CT with some metal-mediated ^{3}ILCT contribution. **1** undergoes a bathochromic shift in color and emission upon grinding (mechanochromism), which is reversed upon fuming the sample with acetone. This behavior is attributed to the shortening of the Pt−Tl separations in the chain induced on grinding. **1** and **2** exhibit blue-shift vapoluminescent responses to donor solvents (THF, Et_2O **1** and Me_2CO, THF, Et_2O **2**) that are larger and faster in the neutral extended chain **1**. The crystal structures of **1**−**3** allowed us to propose an explanation to their different behavior toward solvent vapors. Thus, **1** having a Pt/Tl ratio of 1:1, crystallizes with an acetone molecule, which coordinates weakly to the Tl center. Therefore, its vapochromic behavior is ascribed to the fast exchange of the acetone coordinated to the Tl(I) center by other oxygen donor solvents (THF and Et_2O). It is important to note that solid−vapor reactions involving the exchange of ligands coordinated to metal centers are quite rare.[112−115] Complex **2** forms two pseudopolymorphs in

DOI: 10.1021/acs.inorgchem.5b00083
Inorg. Chem. 2015, 54, 4351−4363

CH_2Cl_2/*n*-hexane (**2a**, **2b**) having CH_2Cl_2 molecules of solvation and the adduct **2·THF** (**2c**) with the THF molecule coordinated to the Tl(I), in THF/*n*-hexane. In this adduct, the Tl−O(THF) bonding interaction [2.630(4) Å] is notably shorter than the Tl−O(acetone) in the chain **1** [2.805(6), 2.720(5) Å], which could explain the slowness of the observed desolvation process. In contrast to the vapoluminescent behavior of **1** and **2**, complex **3** did not show any response to liquid or vapors of donor solvents. This might be due to the smaller void space in the crystal lattice of **3** that would be unable to absorb vapor molecules. Expansion to other chromophore platinum substrates could offer a new approach to molecular materials that exhibit multistimuli responses.

EXPERIMENTAL SECTION

General Comments. Literature methods were used to prepare the starting material $(NBu_4)[Pt(bzq)(C_6F_5)_2]$.[14] C, H, and N analyses, conductivities, and IR and NMR spectra were performed as described elsewhere.[14] Mass spectra were recorded on a Microflex MALDI-TOF Bruker spectrometer operating in the linear and reflector modes using as matrix 1,1-dicyano-4-*tert*-butylphenyl-3-methylbutadiene (DCTB, 10 mg/mL in acetone). The ratio of sample/matrix used was 1/10. The optical absorption spectra were recorded using a Hewlett-Packard 8453 (solution) spectrophotometer in the visible and near-UV ranges. Diffuse reflectance UV−vis data of pressed powder were recorded on a Shimadzu (UV-3600 spectrophotometer with a Harrick Praying Mantis accessory) and recalculated following the Kubelka−Munk function. Emission and excitation spectra were obtained on a PerkinElmer luminescence spectrometer LS 50B and on a Jobin-Ybon Horiba Fluorolog 3−22 Tau-3 spectrofluorimeter, with the lifetime measured in phosphorimeter mode (with an F1−1029 lifetime emission PMT assembly, using a 450W Xe lamp) or with a Datastation HUB-B with a nanoLED controller and software DAS6. The nanoLEDs employed for lifetime measurements were of 450 nm with pulse lengths of 0.8−1.4 ns. The lifetime data were fitted using the Jobin-Yvon software package.

Caution! *Perchlorate salts of metal complexes with organic ligands are potentially explosive. Only small amounts of material should be prepared, and these should be handled with great caution.*

Synthesis of $[\{Pt(bzq)(C_6F_5)_2\}Tl(Me_2CO)]_n$ **(1).** To a solution of $TlPF_6$ (0.142 g, 0.408 mmol) in acetone (15 mL) $(NBu_4)[Pt(bzq)(C_6F_5)_2]$ (0.387 g, 0.408 mmol) was added. After 15 h of stirring, the solution was evaporated to 2 mL, and **1** crystallized. The orange-red solid was filtered off, washed with cold acetone (3 × 1 mL), and vacuum-dried; 0.188 g, 51% yield. Anal. Found (calcd for $C_{28}H_{14}F_{10}NOPtTl$): C, 34.66 (34.68); H, 1.36 (1.46); N, 1.43 (1.44)%. MALDI-TOF (−): *m*/*z* (%) 707 $[Pt(bzq)(C_6F_5)_2]^-$ (100), 1620 $[\{Pt(bzq)(C_6F_5)_2\}_2Tl]^-$ (2). MALDI-TOF (+): *m*/*z* (%) 957 $[Pt(bzq)(C_6F_5)_2Tl(CH_3COCH_3)]^+$ (40), 1116 $[Pt(bzq)(C_6F_5)_2Tl_2]^+$ (12). IR (cm^{-1}): 1633 (w), 1503 (s), 1060 (s), 1042 (s), 944 (s), 833 (s), 821 (s), 779 (m, C_6F_5, X-sensitive vibr.),[116] 774 (m, C_6F_5, X-sensitive vibr.),[116] 763 (s). ^1H NMR (acetone-d_6, 295 K, ppm), δ 8.81 (H2, d, $^3J_{H(2),H(3)}$ = 5.1 Hz, $^3J_{H(2),Pt}$ = 28 Hz), 8.63 (H4, d, $^3J_{H(4),H(3)}$ = 7.8 Hz), 7.88 (H5, d, $^3J_{H(5),H(6)}$ = 8.7 Hz), 7.81 (H6, d, $^3J_{H(6),H(5)}$ = 9.0 Hz), 7.67 (H7, d, $^3J_{H(7),H(8)}$ = 7.8 Hz), 7.59 (H3, dd, $^3J_{H(3),H(4)}$ = 7.8 Hz, $^3J_{H(3),H(2)}$ = 5.1 Hz), 7.42 (H8, dd, $^3J_{H(8),H(7)}$ = 7.8 Hz, $^3J_{H(8),H(9)}$ = 7.2 Hz), 7.30 (H9, d, $^3J_{H(9),H(8)}$ = 7.2 Hz, $^3J_{H(9),Pt}$ = 40 Hz).^{19}F NMR (acetone-d_6, 295 K, ppm), δ −114.6 (*o*-F, d, $^3J_{F,F}$ = 25 Hz, $^3J_{F,Pt}$ = 223 Hz), −117.5 (*o*-F, d, $^3J_{F,F}$ = 17 Hz, $^3J_{F,Pt}$ = 426 Hz), −164.8 (F, br m), −166.9 (F, br m). ^{19}F NMR (acetone-d_6, 193 K, ppm), δ −114.4 (*o*-F, br s), −117.2 (*o*-F, br s), −163.9 (F, br m), −166.0 (F, br m). $^{195}Pt\{^1H\}$ NMR (acetone-d_6, 295 K, ppm), δ −2826 (m). Λ_M (acetone): 48 Ω^{-1} cm^{-2} mol^{-1}.

Synthesis of $[NBu_4][\{Pt(bzq)(C_6F_5)_2\}_2Tl]$ **(2).** To a solution of $TlPF_6$ (0.070 g, 0.200 mmol) in acetone (15 mL) $(NBu_4)[Pt(bzq)(C_6F_5)_2]$ (0.380 g, 0.400 mmol) was added. After 15 h of stirring, the solution was evaporated to 2 mL, and **2** crystallized. The orange solid was filtered off and washed with cold acetone (3 × 1 mL); 0.071 g, 20% yield. Anal. Found (calcd for $C_{66}H_{52}F_{20}N_3Pt_2Tl$): C, 42.97 (42.58); H, 2.70 (2.82); N, 2.14 (2.26)%. MALDI-TOF (−): *m*/*z* (%) 707 $[Pt(bzq)(C_6F_5)_2]^-$ (100). MALDI-TOF (+): *m*/*z* (%) 623 $[Pt(bzq)Tl(CH_3COCH_3)]^+$ (95), 957 $[Pt(bzq)(C_6F_5)_2Tl_2(CH_3COCH_3)]^+$ (100). IR (cm^{-1}): 1633 (w), 1503 (s), 1060 (s), 1042 (s), 944 (s), 833 (s), 821 (s), 779 (m, C_6F_5, X-sensitive vibr.),[116] 774 (m, C_6F_5, X-sensitive vibr.),[116] 763 (s). ^1H NMR (acetone-d_6, 1×10^{-3} M, 298 K, ppm) δ 8.62 (H2, d, $^3J_{H(2),H(3)}$ = 3.5 Hz, $^3J_{H(2),Pt}$ = 28 Hz), 8.54 (H4, d, $^3J_{H(4),H(3)}$ = 7.7 Hz), 7.81 (H5, d, $^3J_{H(5),H(6)}$ = 8.7 Hz), 7.70 (H6, d, $^3J_{H(6),H(5)}$ = 8.5 Hz), 7.60 (H7, d, $^3J_{H(7),H(8)}$ = 7.5 Hz), 7.51 (H3, dd, $^3J_{H(3),H(4)}$ = 6.0 Hz, $^3J_{H(3),H(2)}$ = 5.1 Hz), 7.33 (H8, dd, $^3J_{H(8),H(7)}$ = 7.8 Hz, $^3J_{H(8),H(9)}$ = 6.9 Hz), 7.14 (H9, d, $^3J_{H(9),H(8)}$ = 6.5 Hz, $^3J_{H(9),Pt}$ = 42 Hz), 3.41 (8H, m, $N(C\underline{H}_2CH_2CH_2CH_3)^+$), 1.79 (8H, m, $(N-(CH_2C\underline{H}_2CH_2CH_3)^+$), 1.40 (8H, sext., $(N(CH_2CH_2C\underline{H}_2CH_3)^+$), 0.96 (12H, t, $(N(CH_2CH_2CH_2C\underline{H}_3)^+$). ^{19}F NMR (acetone-d_6, 1×10^{-3} M, 298 K, ppm), δ −114.8 (*o*-F, d, $^3J_{F,F}$ = 25 Hz, $^3J_{F,Pt}$ = 255 Hz), −116.8 (*o*-F, d, $^3J_{F,F}$ = 28 Hz, $^3J_{F,Pt}$ = 500 Hz), −165.5 (*m*-F, br m), −166.0 (*p*-F, t, $^3J_{F,F}$ = 20 Hz), −167.9 (*m*-F, br m), −168.4 (*p*-F, t, $^3J_{F,F}$ = 20 Hz). ^{19}F NMR (acetone-d_6, 1×10^{-3} M, 193 K, ppm), δ −115.9 (*o*-F, br m), −164.3 (*m*-F, br m), −164.6 (*p*-F, br m), −166.7 (*m*-F, br m), −166.9 (*p*-F, br m). $^{195}Pt\{^1H\}$ NMR (acetone-d_6, 295 K, ppm), δ −3052 (m). Λ_M (acetone): 118 Ω^{-1} cm^{-2} mol^{-1}.

Synthesis of $[\{Pt(bzq)(C_6F_5)_2\}_2Pb]$ **(3).** To a solution of $PbClO_4 \cdot 3H_2O$ (0.032 g, 0.079 mmol) in acetone (10 mL) $(NBu_4)[Pt(bzq)(C_6F_5)_2]$ (0.150 g, 0.158 mmol) was added. After 40 min of stirring in absence of light, the solution was evaporated to 2 mL, and **3** crystallized. The yellow-orange solid was filtered off, washed with cold acetone (3 × 1 mL), and vacuum-dried; 0.085 g, 67% yield. Anal. Found (calcd for $C_{50}H_{16}F_{20}N_2Pt_2Pb$): C, 36.81 (37.02); H, 1.23 (0.99); N, 1.74 (1.73)%. MALDI-TOF (+): *m*/*z* (%) 913 $[Pt(bzq)(C_6F_5)_2Pb]^+$ (33), 1454 $[Pt_2(bzq)_2(C_6F_5)_3Pb]^+$ (13). IR (cm^{-1}): 1635(w), 1617(w), 1605(w), 1504(m), 1059(m), 949 (s), 836 (m), 822 (s), 803 (m), 780 (m, C_6F_5, X-sensitive vibr.),[116] 759 (m, C_6F_5, X-sensitive vibr.),[116] 652 (s). ^1H NMR (acetone-d_6, 295 K, ppm), δ 8.61 (H4, d, $^3J_{H(4),H(3)}$ = 7.8 Hz), 8.56 (H2, d, $^3J_{H(2),H(3)}$ = 5.1 Hz, $^3J_{H(2),Pt}$ = 25 Hz), 7.90 (H5, d, $^3J_{H(5),H(6)}$ = 8.7 Hz), 7.83 (H6, d, $^3J_{H(6),H(5)}$ = 9.0 Hz), 7.67 (H7, d, $^3J_{H(7),H(8)}$ = 8.1 Hz), 7.6 (H3, dd, $^3J_{H(3),H(4)}$ = 7.82 Hz, $^3J_{H(3),H(2)}$ = 5.1 Hz), 7.30 (H8, dd, $^3J_{H(8),H(7)}$ = 7.5 Hz, $^3J_{H(8),H(9)}$ = 6.9 Hz), 7.12 (H9, d, $^3J_{H(9),H(8)}$ = 6.9 Hz, $^3J_{H(9),Pt}$ = 38 Hz). ^{19}F NMR (acetone-d_6, 295 K, ppm), δ −115.1 (*o*-F, br d), −118.7 (*o*-F, br d), −163.8 (F, s), −167.4 (F,s), −165.8 (F, s), −166.3 (F,s). Its low solubility prevented characterization by $^{195}Pt\{^1H\}$ NMR spectroscopy. Λ_M (acetone): 35 Ω^{-1} cm^{-2} mol^{-1}.

X-ray Structure Determinations. Crystal data and other details of the structure analyses are presented in Supporting Information, Table S5. Suitable crystals for X-ray diffraction studies were obtained by slow diffusion of *n*-hexane into concentrated solutions of the complexes in 3 mL of Me_2CO (**1**·*x*0.5Me_2CO·*x*0.25*n*-C_6H_{14}, and **3**), CH_2Cl_2 [**2**·0.75CH_2Cl_2 (**2a**), **2**·CH_2Cl_2 (**2b**)], or THF [**2·THF** (**2c**)]. Crystals were mounted at the end of a quartz fiber. The radiation used in all cases was graphite monochromated Mo Kα (λ = 0.710 73 Å). For **1**·*x*0.5Me_2CO·*x*0.25*n*-C_6H_{14}, **2**·0.75CH_2Cl_2, **2**·CH_2Cl_2, and **3**, X-ray intensity data were collected on an Oxford Diffraction Xcalibur diffractometer, and the diffraction frames were integrated and corrected from absorption by using the CrysAlis RED program.[117] For **2·THF**, X-ray intensity data were collected with a NONIUS-κCCD area-detector diffractometer, and images were processed using the DENZO and SCALEPACK suite of programs;[118] the absorption correction was performed using SORTAV.[119]

The structures were solved by Patterson and Fourier methods and refined by full-matrix least-squares on F^2 with SHELXL-97.[120] All non-hydrogen atoms were assigned anisotropic displacement parameters and refined without positional constraints, except as noted below. All hydrogen atoms were constrained to idealized geometries and assigned isotropic displacement parameters equal to 1.2 times the U_{iso} values of their attached parent atoms (1.5 times for the methyl hydrogen atoms).

In the structure of **1**·*x*0.5Me_2CO·*x*0.25*n*-C_6H_{14}, one of the bzq ligands is disordered over two sets of positions, which were refined with partial occupancy of 0.7/0.3. Weak restraints were applied over

DOI: 10.1021/acs.inorgchem.5b00083
Inorg. Chem. 2015, 54, 4351−4363

the geometry of these moieties, and the equivalent atoms of both were refined with common anisotropic displacement parameters. Moreover, a very diffuse molecule of *n*-hexane was found during the refinement, and the occupancy of its atoms was fixed to 0.3. Geometric parameters for this molecule were restrained to acceptable values. For **2**·$0.75CH_2Cl_2$ (**2a**, monoclinic, $P2_1/n$) very diffuse solvent was found in the final stages of the refinement and modeled as two dichloromethane molecules with partial occupancy of 0.50 and 0.75. Geometric parameters for these molecules were restrained to acceptable values. **2**·CH_2Cl_2 (**2b**, monoclinic $P2_1/c$), includes a full CH_2Cl_2 molecule in the asymmetric part of the unit cell. In this, a terminal CH_2-CH_3 fragment of the tetrabutylammonium cation was found to be disordered, and the disorder modeled as two sites with partial occupancy of 0.6/0.4. Constraints were applied on the geometry and the anisotropic displacement parameters of these C atoms. **2·THF** (**2c**, orthorhombic *Pbca*), includes a THF molecule coordinated to the Tl center. In the structure of **3**, some very diffuse and minor electron residual density was present without a clear chemical meaning. After several attempts to model this density as oxygen water atoms, with very low occupancy and not very convincing results, the SQUEEZE procedure as implemented in PLATON[121] was used giving rise to satisfactory results. Full-matrix least-squares refinement of these models against F^2 converged to final residual indices given in Supporting Information, Table S5.

■ ASSOCIATED CONTENT

Supporting Information

Selected bond lengths and angles for compounds **1**·$x0.5Me_2CO$·$x0.25n$-C_6H_{14}, **2**·$0.75CH_2Cl_2$ (**2a**), **2**·CH_2Cl_2 (**2b**), **2**·THF (**2c**), and **3** both in tabular and CIF format; photophysical data for complexes **1**−**3** in solution; tabulated crystallographic structural parameters; illustrated molecular structures; ^{19}F NMR and UV−vis spectra of the complexes described in this paper. This material is available free of charge via the Internet at http://pubs.acs.org.

■ AUTHOR INFORMATION

Corresponding Authors

*E-mail: tello@unizar.es. (A.M.)

*E-mail: teresa.moreno@unirioja.es. (M.T.M.)

Present Address

[§]Dpto. de Química Inorgánica y Orgánica, Universitat Jaume I Avda. Vicente Sos Baynat s/n, 12071, Castellón, Spain.

Notes

The authors declare no competing financial interest.

■ ACKNOWLEDGMENTS

This work was supported by the Spanish MICINN (DGPTC/FEDER) (Project No. CTQ2008-06669-C02-01-02/BQU) and MINECO/FEDER (Projects Nos. CTQ2012-35251 and CTQ2013-45518-P) and the Gobierno de Aragón (Grupo Consolidado E21: Química Inorgánica y de los Compuestos Organometálicos).

■ REFERENCES

(1) Pyykkö, P. *Chem. Rev.* **1997**, *97*, 597−636.
(2) Pyykkö, P. *Angew. Chem., Int. Ed.* **2004**, *43*, 4412−4456.
(3) Gade, L. H. *Angew. Chem., Int. Ed.* **2001**, *40*, 3573−3575.
(4) Carvajal, M. A.; Álvarez, S.; Novoa, J. J. *Chem, Eur. J.* **2004**, *10*, 2117−2132.
(5) Díez, A.; Lalinde, E.; Moreno, M. T. *Coord. Chem. Rev.* **2011**, *255*, 2426−2447.
(6) Fernández, E. J.; Laguna, A.; López de Luzuriaga, J. M. *Dalton Trans.* **2007**, 1969−1981.
(7) Fernández, E. J.; López de Luzuriaga, J. M.; Monge, M.; Rodríguez, M. A.; Crespo, O.; Gimeno, M. C.; Laguna, A.; Jones, P. G. *Chem, Eur. J.* **2000**, *6*, 636−644.
(8) Yam, V. W. W.; Cheng, E. C. C. *Chem. Soc. Rev.* **2008**, *37*, 1806−1813.
(9) Schmidbaur, H.; Schier, A. *Chem. Soc. Rev.* **2008**, *37*, 1931−1951.
(10) Sculfort, S.; Braunstein, P. *Chem. Soc. Rev.* **2011**, *40*, 2741−2760.
(11) Fernández, E. J.; Laguna, A.; López de Luzuriaga, J. M. *Coord. Chem. Rev.* **2005**, *249*, 1423−1433.
(12) Moret, M.-E.; Chen, P. *J. Am. Chem. Soc.* **2009**, *131*, 5675−5690.
(13) Forniés, J.; Ibáñez, S.; Martín, A.; Sanz, M.; Berenguer, J. R.; Lalinde, E.; Torroba, J. *Organometallics* **2006**, *25*, 4331−4340.
(14) Forniés, J.; Ibáñez, S.; Martín, A.; Gil, B.; Lalinde, E.; Moreno, M. T. *Organometallics* **2004**, *23*, 3963−3975.
(15) Yamaguchi, T.; Yamazaki, F.; Ito, T. *J. Am. Chem. Soc.* **1999**, *121*, 7405−7406.
(16) Falvello, L. R.; Forniés, J.; Garde, R.; García, A.; Lalinde, E.; Moreno, M. T.; Steiner, A.; Tomás, M.; Usón, I. *Inorg. Chem.* **2006**, *45*, 2543−2552.
(17) Berenguer, J. R.; Díez, A.; Fernández, J.; Forniés, J.; García, A.; Gil, B.; Lalinde, E.; Moreno, M. T. *Inorg. Chem.* **2008**, *47*, 7703−7716.
(18) Falvello, L. R.; Forniés, J.; Martín, A.; Sicilia, V.; Villarroya, P. *Organometallics* **2002**, *21*, 4604−4610.
(19) Alonso, E.; Forniés, J.; Fortuño, C.; Martín, A.; Orpen, A. G. *Organometallics* **2003**, *22*, 5011−5019.
(20) Rochon, F. D.; Melanson, R. *Acta Crystallogr., Sect. C: Cryst. Struct. Commun.* **1988**, *44*, 474−477.
(21) Forniés, J.; Fuertes, S.; Martín, A.; Sicilia, V.; Gil, B.; Lalinde, E. *Dalton Trans.* **2009**, 2224−2234.
(22) Casas, J. M.; Forniés, J.; Fuertes, S.; Martín, A.; Sicilia, V. *Organometallics* **2007**, *26*, 1674−1685.
(23) Falvello, L. R.; Forniés, J.; Fortuño, C.; Durán, F.; Martín, A. *Organometallics* **2002**, *21*, 2226−2234.
(24) Ara, I.; Falvello, L. R.; Forniés, J.; Gómez, J.; Lalinde, E.; Merino, R. I.; Usón, I. *J. Organomet. Chem.* **2002**, *663*, 284−288.
(25) Falvello, L. R.; Forniés, J.; Lalinde, E.; Menjón, B.; García Monforte, M. A.; Moreno, M. T.; Tomás, M. *Chem. Commun.* **2007**, 3838−3840.
(26) Yamaguchi, T.; Yamazaki, F.; Ito, T. *J. Am. Chem. Soc.* **2001**, *123*, 743−744.
(27) Forniés, J.; Ibáñez, S.; Lalinde, E.; Martín, A.; Moreno, M. T.; Tsipis, A. C. *Dalton Trans.* **2012**, *41*, 3439−3451.
(28) Fuertes, S.; Woodall, C. H.; Raithby, P. R.; Sicilia, V. *Organometallics* **2012**, *31*, 4228−4240.
(29) Belío, Ú.; Fuertes, S.; Martín, A. *Inorg. Chem.* **2013**, *52*, 5627−5629.
(30) Martín, A.; Belío, U.; Fuertes, S.; Sicilia, V. *Eur. J. Inorg. Chem.* **2013**, 2231−2247.
(31) Chou, P. T.; Chi, Y. *Chem.—Eur. J.* **2007**, *13*, 380−395.
(32) Cooke, M. W.; Hanan, G. S. *Chem. Soc. Rev.* **2007**, *36*, 1466−1476.
(33) Evans, R. C.; Douglas, P.; Wiscom, C. J. *Coord. Chem. Rev.* **2006**, *250*, 2093−2126.
(34) Holder, E.; Langeveld, B. M. W.; Schubert, U. S. *Adv. Mater.* **2005**, *17*, 1109−1121.
(35) McClenaghan, M. D.; Leydet, N. D.; Maubert, Y.; Indelli, M. T.; Campagna, S. *Coord. Chem. Rev.* **2005**, *249*, 1336−1350.
(36) Sun, S. S.; Lees, A. J. *Coord. Chem. Rev.* **2002**, *230*, 171−192.
(37) Wong, W. Y. *Comments Inorg. Chem.* **2005**, *26*, 39−74.
(38) Huynh, M. H. V.; Dattelbaum, D. M.; Meyer, T. J. *Coord. Chem. Rev.* **2005**, *249*, 457−483.
(39) Vogler, A.; Kunkely, H. *Top. Curr. Chem.* **2001**, *213*, 143−182.
(40) Thanasekaran, P.; Liao, R. T.; Liu, Y. H.; Rajendran, T.; Rajagopal, S.; Lu, K. L. *Coord. Chem. Rev.* **2005**, *249*, 1085−1110.
(41) *Coord. Chem. Rev.* **2000**, *208* (special issue), 1−371.
(42) Ma, B.; Djurovich, P. I.; Thompson, M. E. *Coord. Chem. Rev.* **2005**, *249*, 1501−1510 and references therein.

DOI: 10.1021/acs.inorgchem.5b00083
Inorg. Chem. 2015, 54, 4351−4363

(43) Pérez, S.; López, C.; Caubet, A.; Bosque, R.; Solans, X.; Bardía, M. F.; Roig, A.; Molins, E. *Organometallics* **2004**, *23*, 224−236 and references therein.
(44) Kobayashi, A.; Kato, M. *Eur. J. Inorg. Chem.* **2014**, *2014*, 4469−4483.
(45) Wenger, O. S. *Chem. Rev.* **2013**, *113*, 3686−3733.
(46) Zhang, X.; Li, B.; Chen, Z.-H.; Chen, Z.-N. *J. Mater. Chem.* **2012**, *22*, 11427−11441.
(47) Zhao, Q.; Li, F.; Huang, C. *Chem. Soc. Rev.* **2010**, *39*, 3007−3030.
(48) Berenguer, J. R.; Lalinde, E.; Martín, A.; Moreno, M. T.; Ruiz, S.; Sánchez, S.; Shahsavari, H. R. *Inorg. Chem.* **2014**, *53*, 8770−8785.
(49) Forniés, J.; Martín, A. In *Metal Clusters in Chemistry;* Braunstein, P., Oro, L. A., Raithby, P. R., Eds.; Wiley-VCH: Weinheim, Germany, 1999; Vol. *1*, pp 417−443.
(50) Forniés, J.; Fortuño, C.; Ibáñez, S.; Martín, A. *Inorg. Chem.* **2008**, *47*, 5978−5987.
(51) Forniés, J.; Gómez, J.; Lalinde, E.; Moreno, M. T. *Inorg. Chem.* **2001**, *40*, 5415−5419.
(52) Casas, J. M.; Forniés, J.; Martín, A.; Menjón, B.; Tomás, M. *Polyhedron* **1996**, *15*, 3599−3604.
(53) Chen, W.; Liu, F.; Nishioka, T.; Matsumoto, K. *Eur. J. Inorg. Chem.* **2003**, 4234−4243.
(54) Díez, A.; Forniés, J.; Gómez, J.; Lalinde, E.; Martín, A.; Moreno, M. T.; Sánchez, S. *Dalton Trans.* **2007**, 3653−3660.
(55) Kampf, G.; Miguel, P. J. S.; Willermann, M.; Schneider, A.; Lippert, B. *Chem.—Eur. J.* **2008**, *14*, 6882−6891.
(56) Song, H. B.; Zhang, Z.-Z.; Hui, Z.; Che, C.-M.; Mak, T. C. W. *Inorg. Chem.* **2002**, *41*, 3146−3154.
(57) Janzen, D. E.; Mehne, L. F.; VanDerveer, D. G.; Grant, G. J. *Inorg. Chem.* **2005**, *44*, 8182−8184.
(58) Baudron, S. A.; Hosseini, M. W. *Chem. Commun.* **2008**, 4558−4560.
(59) Yin, G.-Q.; Wei, Q.-H.; Zhang, L.-Y.; Chen, Z.-N. *Organometallics* **2006**, *25*, 580−587.
(60) Xia, B.-H.; Zhang, H.-X.; Che, C.-M.; Leung, K.-H.; Phillips, D.-L.; Zhu, N.; Zhou, Z.-Y. *J. Am. Chem. Soc.* **2003**, *125*, 10362−10374.
(61) Moret, M.-E.; Chen, P. *Organometallics* **2008**, *27*, 4903−4916.
(62) Ara, I.; Falvello, L. R.; Forniés, J.; Sicilia, V.; Villarroya, P. *Organometallics* **2000**, *19*, 3091−3099.
(63) Ara, I.; Forniés, J.; Sicilia, V.; Villarroya, P. *Dalton Trans.* **2003**, 4238−4242.
(64) Usón, R.; Forniés, J.; Tomás, M.; Garde, R.; Alonso, P. J. *J. Am. Chem. Soc.* **1995**, *117*, 1837−1838.
(65) Baya, M.; Belío, Ú.; Forniés, J.; Martín, A.; Perálvarez, M.; Sicilia, V. *Inorg. Chim. Acta* **2015**, *424*, 136−149.
(66) Usón, R.; Forniés, J.; Tomás, M.; Garde, R.; Merino, R. *Inorg. Chem.* **1997**, *36*, 1383−1387.
(67) Balch, A. L.; Rowley, S. P. *J. Am. Chem. Soc.* **1990**, *112*, 6139−6140.
(68) Oberbeckmann-Winter, N.; Braunstein, P.; Welter, R. *Organometallics* **2004**, *23*, 6311−6318.
(69) Nagle, J. K.; Balch, A. L.; Olmstead, M. M. *J. Am. Chem. Soc.* **1988**, *110*, 319−321.
(70) Charmant, J. P. H.; Forniés, J.; Gómez, J.; Lalinde, E.; Merino, R. I.; Moreno, M. T.; Orpen, A. G. *Organometallics* **2003**, *22*, 652−656.
(71) Liu, F.; Chen, W.; Wang, D. *Chin. J. Struct. Chem.* **2006**, *25*, 677−680.
(72) Berenguer, J. R.; Fernández, J.; Lalinde, E.; Sánchez, S. *Chem. Commun.* **2012**, *48*, 6384−6386.
(73) Renn, O.; Lippert, B.; Mutikainen, I. *Inorg. Chim. Acta* **1993**, *208*, 219−223.
(74) Chen, W.; Liu, F.; Xu, D. X.; Matsumoto, K.; Kishi, S.; Kato, M. *Inorg. Chem.* **2006**, *45*, 5552−5560.
(75) Stork, J. R.; Olmstead, M. M.; Fettinger, J. C.; Balch, A. L. *Inorg. Chem.* **2006**, *45*, 849−857.
(76) Forniés, J.; García, A.; Lalinde, E.; Moreno, M. T. *Inorg. Chem.* **2008**, *47*, 3651−3660.
(77) Stork, J. R.; Olmstead, M. M.; Balch, A. L. *J. Am. Chem. Soc.* **2005**, *127*, 6512−6513.
(78) Díez, A.; Fernández, J.; Lalinde, E.; Moreno, M. T.; Sánchez, S. *Inorg. Chem.* **2010**, *49*, 11606−11618.
(79) Belío, Ú.; Fuertes, S.; Martín, A. *Dalton Trans.* **2014**, *43*, 10828−10843.
(80) Berenguer, J. R.; Forniés, J.; Gil, B.; Lalinde, E. *Chem.—Eur. J.* **2006**, *12*, 785−795.
(81) Wu, G.; Wang, D. *J. Cluster Sci.* **2007**, *18*, 406−413.
(82) Balch, A. L.; Fung, E. Y.; Nagle, J. K.; Olmstead, M. M.; Rowley, S. P. *Inorg. Chem.* **1993**, *32*, 3295−3299.
(83) Usón, R.; Forniés, J.; Falvello, L. R.; Usón, M. A.; Usón, I. *Inorg. Chem.* **1992**, *31*, 3697−3698.
(84) Albano, V. G.; Castellari, C.; Monari, M.; DeFelice, V.; Ferrara, M. L.; Ruffo, F. *Organometallics* **1995**, *14*, 4213−4221.
(85) Casas, J. M.; Forniés, J.; Martín, A.; Orera, V. M.; Orpen, A. G.; Rueda, A. *Inorg. Chem.* **1995**, *34*, 6514−6519.
(86) Berenguer, J. R.; Fernández, J.; Gil, B.; Lalinde, E.; Sánchez, S. *Chem.—Eur. J.* **2014**, *20*, 2574−2584.
(87) Berenguer, J. R.; Lalinde, E.; Martín, A.; Moreno, M. T.; Ruiz, S.; Sánchez, S.; Shahsavari, H. R. *Chem. Commun.* **2013**, *49*, 5067−5069.
(88) Shimoni-Livny, L.; Glusker, J. P.; Bock, C. W. *Inorg. Chem.* **1998**, *37*, 1853−1867.
(89) Davidovich, R. L.; Stavila, V.; Marinin, D. V.; Voit, E. I.; Whitmire, K. H. *Coord. Chem. Rev.* **2009**, *253*, 1316−1352.
(90) Davidovich, R. L.; Stavila, V.; Whitmire, K. H. *Coord. Chem. Rev.* **2010**, *254*, 2193−2226.
(91) Gourlaouen, C.; Gérard, H.; Piquemal, J.-P.; Parisel, O. *Chem.—Eur. J.* **2008**, *14*, 2730−2743.
(92) Greer, B. J.; Michaelis, V. K.; Katz, M. J.; Leznoff, D. B.; Schreckenbach, G.; Kroeker, S. *Chem.—Eur. J.* **2011**, *17*, 3609−3618.
(93) Jamali, S.; Ghazfar, R.; Lalinde, E.; Jamshidi, Z.; Samouei, H.; Shahsavari, H. R.; Moreno, M. T.; Escudero-Adan, E.; Benet-Buchholz, J.; Milic, D. *Dalton Trans.* **2014**, *43*, 1105−1116.
(94) Ara, I.; Berenguer, J. R.; Forniés, J.; Gómez, J.; Lalinde, E.; Martín, A.; Merino, R. *Inorg. Chem.* **1997**, *36*, 6461−6464.
(95) Bondi, A. *J. Phys. Chem.* **1964**, *68*, 441.
(96) Fernández, E. J.; Laguna, A.; López de Luzuriaga, J. M.; Mendizábal, F.; Monge, M.; Olmos, M. E.; Pérez, J. *Chem.—Eur. J.* **2003**, *9*, 456−465.
(97) Braga, D.; Grepioni, F. *Chem. Soc. Rev.* **2000**, *29*, 229−238.
(98) Fernández, E. J.; López de Luzuriaga, J. M.; Monge, M.; Montiel, M.; Olmos, M. E.; Pérez, J.; Laguna, A.; Mendizábal, F.; A, M. A.; Fackler, J. P. *Inorg. Chem.* **2004**, *43*, 3573−3581.
(99) de Silva, N.; Fry, C. G.; Dahl, L. F. *Dalton Trans.* **2006**, 1051−1059.
(100) Childress, M. V.; Millar, D.; Alam, T. M.; Kreisel, K. A.; Yap, G. P. A.; Zakharov, L. N.; Golen, J. A.; Rheingold, A. L.; Doerrer, L. H. *Inorg. Chem.* **2006**, *45*, 3864−3877.
(101) Dick, A. R.; Kampf, J. W.; Sanford, M. S. *Organometallics* **2005**, *24*, 482−485.
(102) De Priest, J.; Zheng, G. Y.; Woods, C.; Rillema, D. P.; Mikirova, N. A.; Zandler, M. E. *Inorg. Chim. Acta* **1997**, *264*, 287−296.
(103) Godbert, N.; Pugliese, T.; Aiello, I.; Bellusci, A.; Crispini, A.; Ghedini, M. *Eur. J. Inorg. Chem.* **2007**, 5105−5111.
(104) Díez, A.; Forniés, J.; García, A.; Lalinde, E.; Moreno, M. T. *Inorg. Chem.* **2005**, *44*, 2443−2453.
(105) Jolliet, P.; Gianini, M.; von Zelewsky, A.; Bernardinelli, G.; Stoeckli-Evans, H. *Inorg. Chem.* **1996**, *35*, 4883−4888.
(106) Janzen, D. E.; VanDerveer, D. G.; Mehne, L. F.; da Siva Filho, D. A.; Bredas, J. L.; Grant, G. J. *Dalton Trans.* **2008**, 1872−1882.
(107) Shannon, R. D. *Acta Crystallogr.* **1976**, *A32*, 751−767.
(108) Dolg, M.; Pyykkö, P.; Runeberg, N. *Inorg. Chem.* **1996**, *35*, 7450−7451.
(109) Houlding, V. H.; Miskoswski, V. M. *Coord. Chem. Rev.* **1991**, *111*, 145−152.
(110) Zheng, G. Y.; Rillema, D. P. *Inorg. Chem.* **1998**, *37*, 1392−1397.

DOI: 10.1021/acs.inorgchem.5b00083
Inorg. Chem. 2015, 54, 4351−4363

(111) Forniés, J.; Fuertes, S.; Martín, A.; Sicilia, V.; Lalinde, E.; Moreno, M. T. *Chem.—Eur. J.* **2006**, *12*, 8253.
(112) Strasser, C. E.; Catalano, V. J. *J. Am. Chem. Soc.* **2010**, *132*, 10009−10011.
(113) Ley, A. N.; Dunaway, L. E.; Brewster, T. P.; Dembo, M. D.; Harris, T. D.; Baril-Robert, F.; Li, X.; Patterson, H. H.; Pike, R. D. *Chem. Commun.* **2010**, *46*, 4565−4567.
(114) Supriya, S.; Das, S. K. *J. Am. Chem. Soc.* **2007**, *129*, 3464−3465.
(115) Lefebvre, J.; Korcok, J. L.; Katz, M. J.; Leznoff, D. B. *Sensors* **2012**, *12*, 3669−3692.
(116) Maslowsky, E. J. *Vibrational Spectra of Organometallic Compounds;* Wiley: New York, 1977.
(117) *CrysAlis RED,* CCD camera data reduction program; Oxford Diffraction: Oxford, U.K., 2004.
(118) Otwinowski, Z.; Minor, W. *Methods Enzymol.* **1997**, *276*, 307−326.
(119) Blessing, R. H. *Acta Crystallogr.* **1995**, *A51*, 33−38.
(120) Sheldrick, G. M. *Acta Crystallogr.* **2008**, *A64*, 112−122.
(121) Spek, A. L. *PLATON, A Multipurpose Crystallographic Tool;* Utrecht University: Utrecht, the Netherlands, 2010.

DOI: 10.1021/acs.inorgchem.5b00083
Inorg. Chem. 2015, 54, 4351−4363